CHAPTER 4

Preliminary Analysis of Strong Ground Motion Characteristics

By:

Zeynep Gülerce [(a), *], Ayşegül Askan [(b)], Özkan Kale [(c)], Abdullah Sandıkkaya [(d)], Nihat Sinan Işık [(e)], Okan İlhan [(f)], Gizem Can [(g)], Makbule Ilgaç [(h)], A. Arda Ozacar [(b)], Eyüp Sopacı [(b)], Kemal Önder Çetin [(b)]

Burak Akbaş [(b), (i)], Abdullah Altındal [(b)], Baran Guryuva[(d)], Onur Kanun [(b)], Kubilay Albayrak [(b)], Gamze Muratoglu [(b)], Oguz Salih Okcu[(d)], Abdullah Icen[(j)], Mehmet Firat Aydin [(b)]

(a) Middle East Technical University (METU, Ankara), currently in International Atomic Energy Agency (IAEA, Vienna)
(b) Middle East Technical University (METU), Ankara
(c) TED University, Ankara
(d) Hacettepe University, Ankara
(e) Gazi University, Ankara
(f) Yildirim Beyazit University, Ankara
(g) Royal Haskoning DHV Resilience & Maritime Netherlands-BL Maritime & Water
(h) University of California, Berkeley
(i) Atilim University, Ankara
(j) Munzur Universitesi, Tunceli

Table of Contents

List of Figures

List of Tables

4.1. Introduction

The mainshocks of February 6, 2023 M_w=7.7 Kahramanmaras-Pazarcik and M_w=7.5 Elbistan earthquakes and their aftershock sequences were recorded in a large region by the strong motion stations operated by AFAD (Disaster and Emergency Presidency of Turkey). The recordings and station metadata are disseminated through AFAD's website, soon after both earthquakes (1st event at https://tadas.afad.gov.tr/event-detail/15499 and 2nd event at https://tadas.afad.gov.tr/event-detail/15512, last accessed on February 12, 2023). The reconnaissance team downloaded the raw strong motion data immediately after they were available. However, sharing the responsibility of providing accurate data sets to the scientific and earthquake engineering community, updates in data by AFAD's personnel are being carefully monitored and changes have been implemented in this report as much as possible. It is clear that these recordings are currently evaluated by AFAD and improvements in data quality are expected in near future. The locations of strong ground motion stations in Türkiye are shown in Figure 4.1.

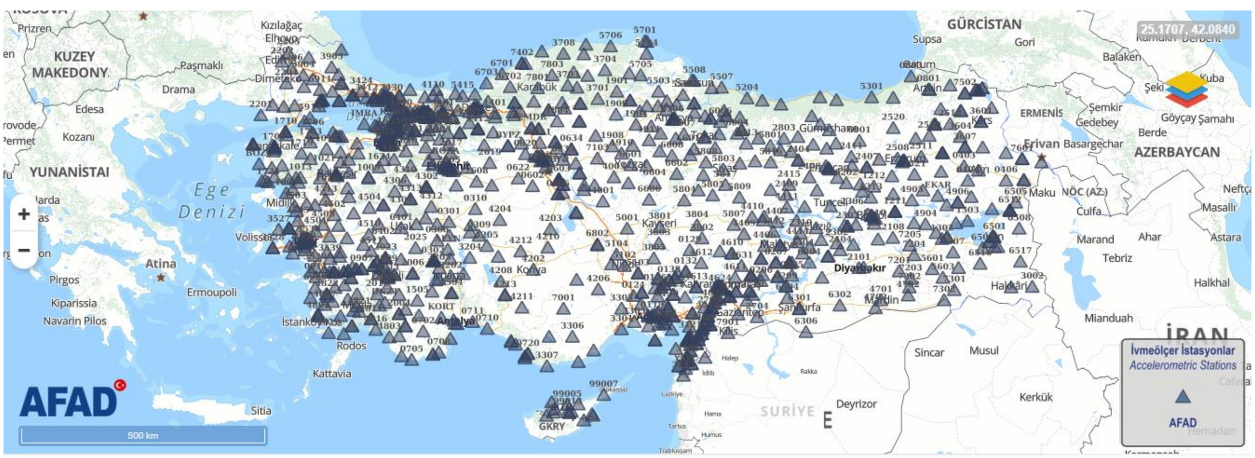

Figure 4.1. The locations of strong ground motion stations in Türkiye (AFAD-TADAS)

For this preliminary report, 292 and 268 three-component recordings from the first and second event, respectively, were compiled, analyzed for data quality, and processed as summarized in Section 4.2. Further assessments, including the analysis of spectral shapes and amplifications, comparisons with design envelopes and mean predictions of current ground motion models were performed by using data that passed the quality check. Therefore, this chapter aims to present only the current state of factual information on the strong motion characteristics of these very important events. With this report, we state that we have no intention or authorization to disseminate the strong motion data that is owned by the national network.

Our objective is to offer several ground motion intensity measures (GMIMs) that may be used for the analysis of structural and geotechnical performance of structures during the February 6, 2023 earthquakes. Therefore, several amplitude and intensity parameters (peak accelerations, peak and cumulative absolute velocities, Arias and Housner intensities, etc.), significant duration, Fourier Amplitude and response spectrums for 5% damping are provided in this report. Important GMIMs are also disseminated through the SiteEye Software (https://siteeye.co). The metadata for stations, including the shear wave velocity profiles and the extended source-to-site distance metrics, are carefully evaluated with the current state of available information. As the geological reconnaissance efforts progress, the extent of rupture will be more accurately defined. This may change some of the initial interpretations given in this report, especially for the recordings collected from both ends of the rupture.

4.2. Quality Control and Strong Motion Data Processing

The strong motion database used in this report mainly consists of data disseminated by the AFAD-TADAS website between February 6-10, 2023. However, some recordings were updated in the system on February 12-13, 2023, which were also utilized in this report. The "freezing date" for data compilation was set as February 13, 2023 to ensure timely publication of the report and any changes made after the freezing date were not implemented in the analyses.

4.2.1. Visual Checks on the Waveform Data

Collected (raw) waveforms underwent an initial visual screening to identify non-standard errors, as defined by Douglas (2003) and Boore and Bommer (2005). Since the rupture propagation of the first event was bilateral, with directions towards Kahramanmaras in the northeast and Hatay in the southwest, most waveforms included multiple wave packets. The recorded time series initially included the wave packets from the northeast-oriented rupture of the Pazarcik segment, followed by the southwest-oriented rupture of the Amanos segment, which slightly overlapped with the first. The time lag between these multiple wave packets was sometimes visible, as shown in Figure 4.2(a), but varied significantly depending on the station location. Due to the difficulty of separating these wave packets in most stations without finite fault modelling (e.g. Figure 4.2b); we did not attempt to perform waveform analysis or eliminate these recordings from the database. However, we used the entire time history in the evaluation of ground motion intensity measures.

On the other hand, some recordings do not show a clear shape of a seismic waveform, as shown in Figure 4.3(c). These recordings were eliminated from the database during visual screening. Unfortunately, almost all recordings from the stations in Adiyaman province had an incomplete trace of the main event, as shown in Figure 4.3(a) and were excluded from the dataset for this report. We anticipate that AFAD may recompile these recordings from the equipment at a later stage. In addition to the multiple wave groups and incomplete trace problems, some recordings had significant noise content that standard processing could not eliminate (e.g. Figure 4.3b), while others had spikes or were disconnected during the event (e.g. Figure 4.3d). Many recordings had a combination of these problems and were also excluded from the dataset during visual processing.

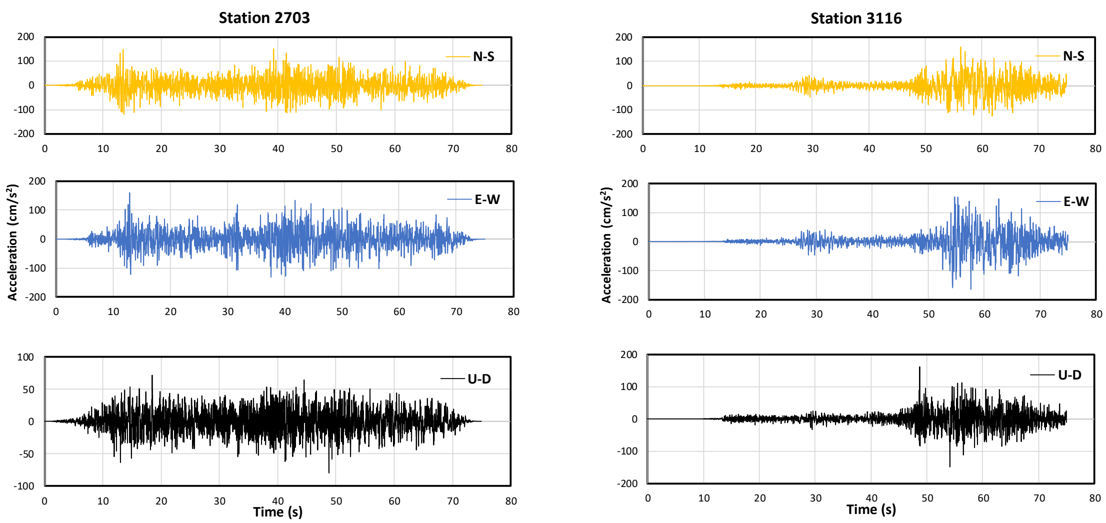

Figure 4.2. A sample acceleration-time history set from Stations ID# 2703 and 3116

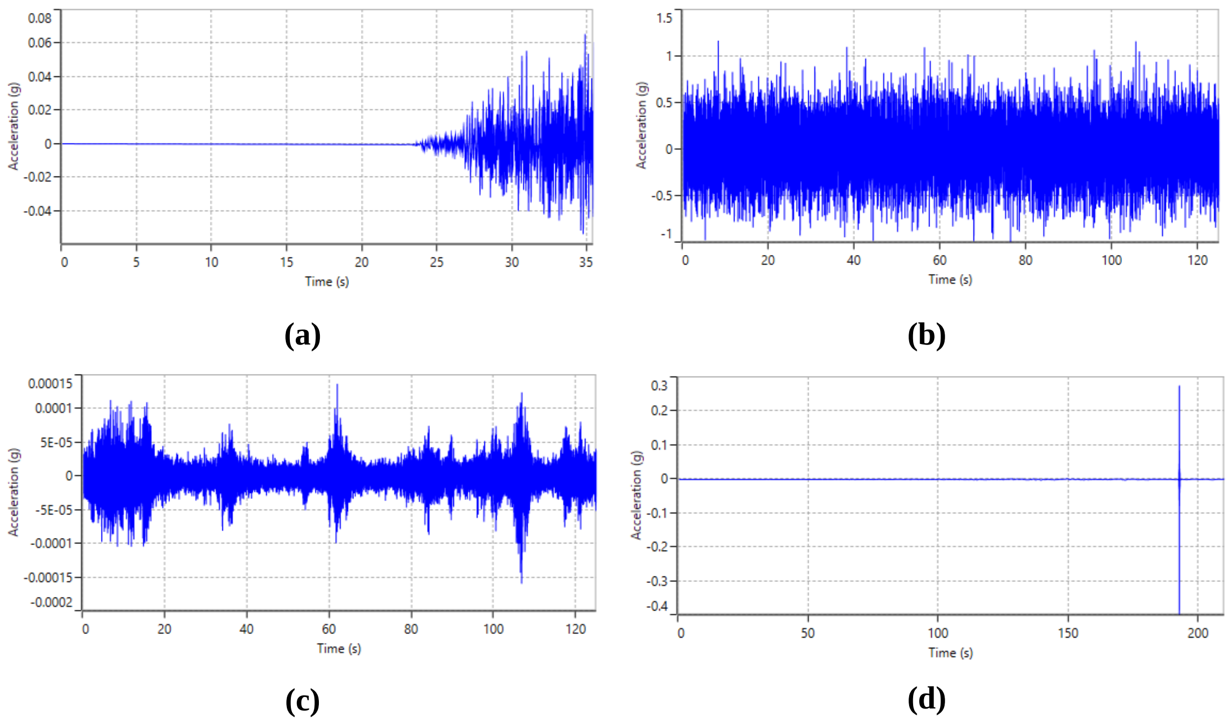

Figure 4.3. Samples for non-standard errors (a) incomplete trace, Station ID# 0210, (b) significant noise content, ID# 3117, (c) unclear trace of event, ID# 3113 and (d) spike, ID# 0719.

4.2.2. Data Processing

After the visual screening, the non-standard, error-free records were processed using the procedures defined in Akkar et al. (2014). First, the zero-ordered correction, which removes the mean acceleration value from the entire waveform, was applied. Next, the low- and high-filter cut-off frequencies were determined by visually inspecting the Fourier Amplitude Spectrum (FAS), velocity, and displacement time series of each waveform (Boore and Bommer, 2005; Douglas and Boore, 2011) as shown in Figure 4.4. An acausal 4-pole Butterworth band-pass filter was used to remove any phase distortion in the signal. Finally, the post processing procedure described in Boore et al. (2012) was used to remove zero pads during band-pass filtering. Most of the low-cut values chosen for the records are below the magnitude-dependent corner frequency of the theoretical source spectrum proposed by Atkinson and Silva (2000) to ensure that the low-frequency motions are retained in the waveforms.

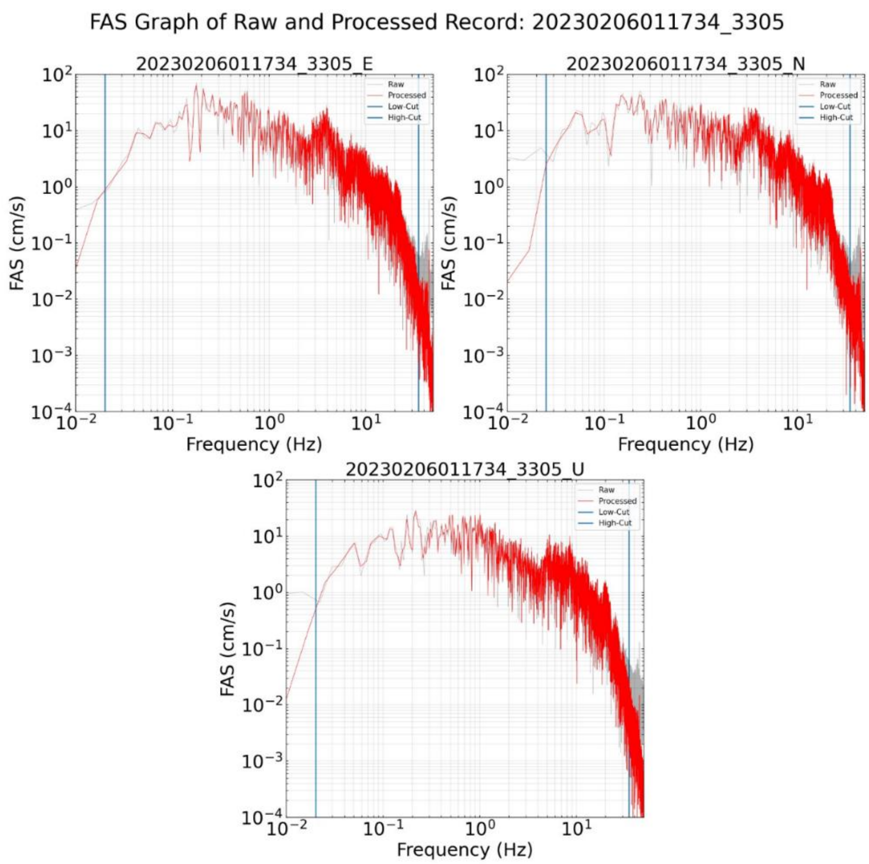

Figure 4.4. FAS of the raw and processed waveforms. The blue solid lines show the low- and high-cut filter frequencies.

4.3. Ground Motion Intensity Measures

Following visual quality control and data processing, 245 recordings from the first earthquake and 244 recordings from the second earthquake remained in the database. Figures 4.5(a) and (b) display the spatial distribution of these recordings for each event, respectively. Additionally, Figure 4.5 shows epicenters (represented by yellow stars) and the surface projections of the estimated rupture planes for each earthquake (for details, please refer to Chapter 3). The extended source-to-site-distance metrics, including rupture distance R_{RUP} and Joyner-Boore distance, R_{JB} were estimated using the procedure given in Kaklamanos et al. (2011) based on these tentative rupture plane parameters. It is worth noting that the depth to the top of the rupture (Z_{TOR}) is assumed to be zero since the rupture is clearly visible at the surface. The fault plane angles are provided in Chapter 3.

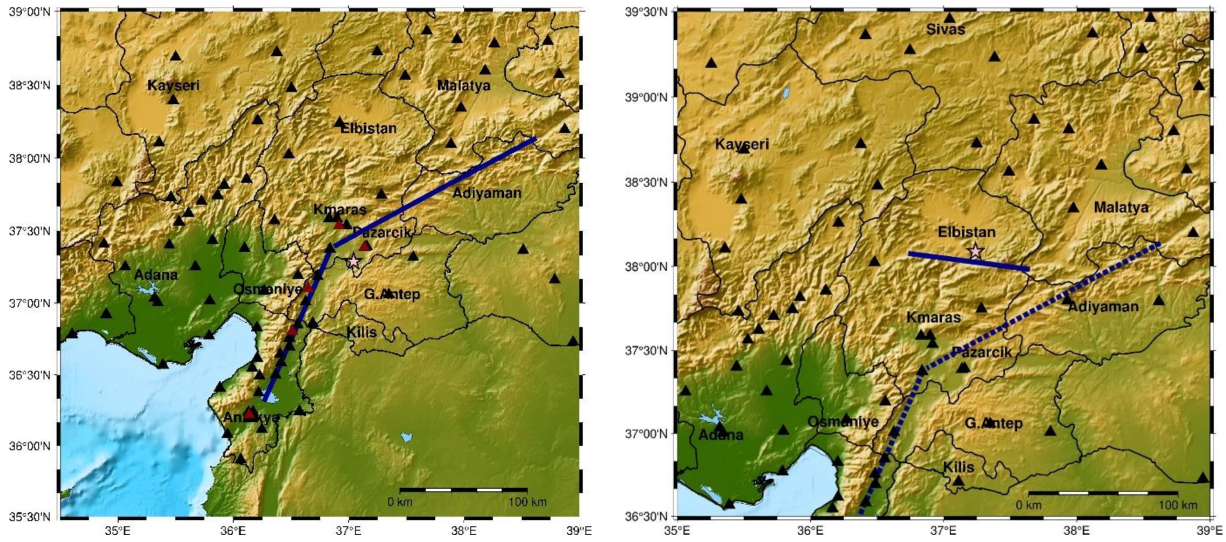

(a) (b)

Figure 4.5. Distribution of the strong motion stations that are located within 200km of the rupture plane for (a) Mw=7.7 Kahramanmaras-Pazarcik and (b) Mw=7.5 Elbistan earthquakes.

For the first event, the V_{S30} (time-averaged shear wave velocity in the upper 30m) information is available for 185 stations. Geophysical methods (MASW and ReMi) were used to measure Vs at141 and 111 recording stations, respectively. Herein, the consistency of V_{S30} values available on AFAD-TADAS website was re-evaluated using site characterization reports. For 9 stations (Station ID: 125, 603, 3133, 3144, 4614, 4628, 5804, 6302, and 3113), the V_{S30} computed from Vs profile provided in the report (based on MASW) was adopted instead of the values given on the AFAD-TADAS website. For the remaining 44 stations, V_{S30} values in AFAD's database were estimated using the topographic slope proxy parameter, as site characterization reports were not available.

For the second earthquake, V_{S30} values were reported for 164 stations on the AFAD-TADAS website, with MASW and ReMi measurements available for 143 and 91 stations, respectively. A similar verification of V_{S30} values was performed, and the V_{S30} information from MASW measurements for 6 stations (Station ID: 603, 3144, 4614, 6302, 4628, and 5804) was adopted.

Figure 4.6 and 4.7 shows the R_{RUP} – V_{S30} distributions of the recordings from the first and second events, respectively. For both events, majority of the stations are located on sites with ZC class according to TBEC (2019). Please note that the site classification scheme of TBEC (2019) is quite similar to that of ASCE 7-19. The remaining stations are classified as ZD or ZB, and there are no stations with V_{S30} < 180 m/s (ZE). The number of near-fault stations (R_{RUP} < 10 km) is significant for the first earthquake but limited for the second earthquake. For both events, ~70% of the stations are located at rupture distances greater than 100 km.

Peak ground motion amplitudes, significant duration, and Arias as well as Housner intensity values of these recordings within R_{RUP}<100km are provided in Table 4.1 and 4.2. In these tables, PGA, and PGV are the peak ground acceleration and velocity, and CAV is the cumulative absolute velocity. The significant duration is calculated as the time between 5% and 95% of the cumulative Arias Intensity. Acceleration time histories, Fourier amplitude spectra and the 5%-damped acceleration response spectra of the recorded accelerations at these stations are provided in Appendix A and a few examples are provided in Figures 4.8 – 4.12 for further discussion. The 5%-damped acceleration response spectra in these figures are compared against the design spectra defined in the current seismic code of Turkey (TBEC, 2019) for 475 and 2475 year return periods.

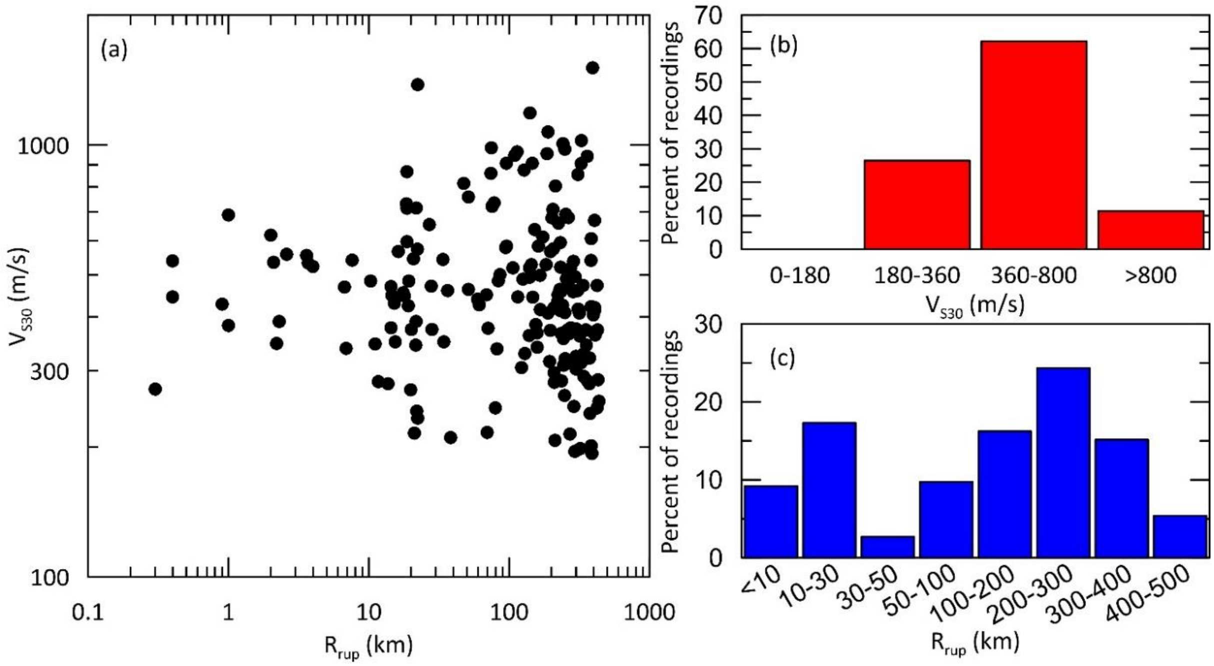

Figure 4.6. (a) R_{RUP} -V_{S30} distribution of the stations in the database, (b) percentage of recording stations in each site class defined in TBEC (2019), and (c) percentage of recording stations in each distance bin (Kahramanmaras/Pazarcik earthquake with M_W=7.7).

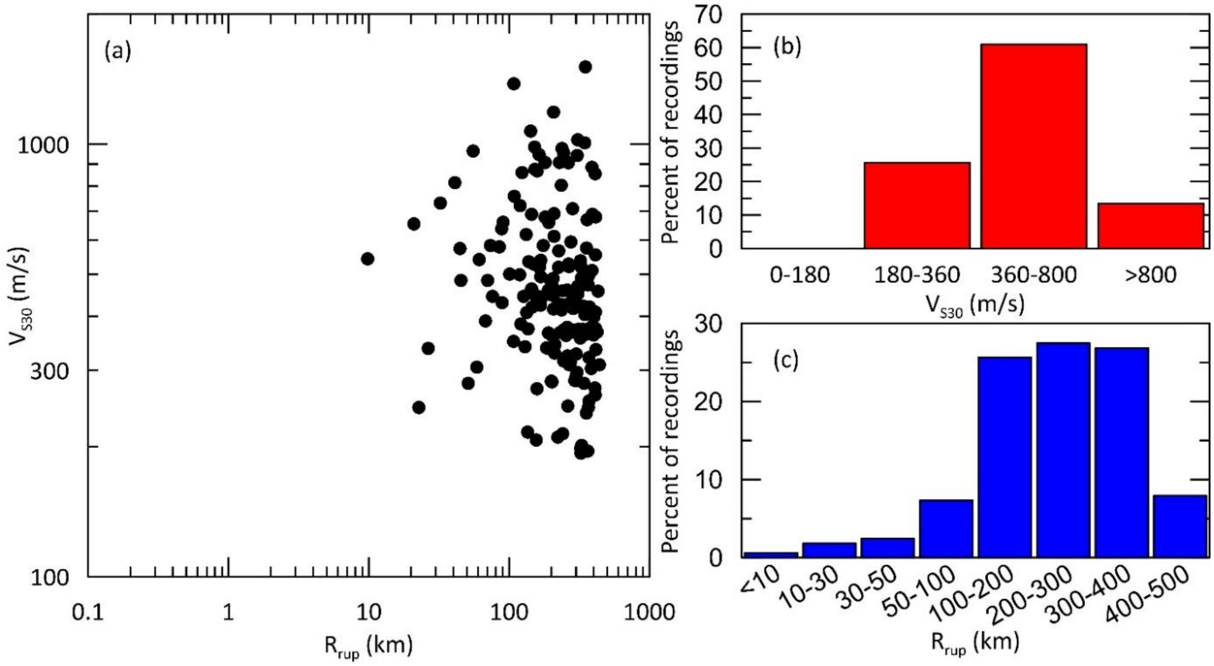

Figure 4.7. R_{RUP} -V_{S30} distribution of the stations in the database, (b) percentage of recording stations in each site class defined in TBEC (2019), and (c) percentage of recording stations in each distance bin (Elbistan earthquake with M_W=7.5).

Table 4.1. Information on Recorded Strong Ground Motions of Pazarcik earthquake for stations within 100 km rupture distance (unknown V_{S30}/Site Class values are shown with NA)

Station Code	City	District	Lat.	Long.	R_{rup}(km)	V_{S30} (m/s)	Site Class*	Comp.	PGA (cm/s^2)	PGV (cm/s)	Significant Duration (s)	Arias Intensity (cm/s)	Housner Intensity (cm)	Cumulative Absolute Velocity (cm/s)
119	Adana	Karataş	36.5680	35.3900	83.80	485	ZC	E-W	44.340	19.01	46.72	9.82	32.62	519.19
								N-S	42.835	8.48	58.2	6.51	20.73	442.90
								U-D	25.275	10.41	63.94	3.84	18.92	356.94
120	Adana	Yumurtalık	36.7701	35.7901	59.60	439	ZC	E-W	115.866	24.82	57.05	42.49	48.39	1034.78
								N-S	112.469	33.93	56.51	42.89	62.43	1051.25
								U-D	103.266	13.14	54.74	13.77	26.65	613.47
122	Adana	Kozan	37.4339	35.8202	86.10	501	ZC	E-W	52.378	8.32	52.43	15.09	20.16	666.06
								N-S	57.323	13.00	52.06	15.21	22.66	666.19
								U-D	33.184	8.94	51.44	4.73	17.19	368.11
125	Adana	Ceyhan	37.0152	35.7958	69.80	216	ZD	E-W	83.225	26.62	60.04	49.21	67.31	1216.86
								N-S	128.556	33.14	60.51	71.87	91.53	1377.95
								U-D	35.141	8.99	60.69	8.70	29.78	536.04
127	Adana	Feke	37.8162	35.9204	95.80	583	ZC	E-W	50.876	4.50	45.5	14.82	15.09	632.92
								N-S	55.088	8.21	41.62	12.79	18.90	550.08
								U-D	39.237	7.51	44.94	4.63	15.62	351.01
130	Adana	İmamoğlu	37.2519	35.6710	90.30	NA	NA	E-W	68.272	14.40	61.76	20.72	43.12	796.49
								N-S	81.197	17.33	55.05	25.44	53.69	856.36
								U-D	35.334	8.28	62.99	7.89	25.56	524.20
131	Adana	Saimbeyli	37.8566	36.1153	84.70	NA	NA	E-W	159.420	6.73	41.93	74.79	12.87	1360.83
								N-S	146.618	7.06	42.53	75.98	15.64	1383.10
								U-D	50.274	7.42	45.19	8.38	13.12	477.19
132	Adana	Saimbeyli	37.8559	36.1149	84.70	NA	NA	E-W	32.476	4.68	47.92	5.27	14.02	382.34
								N-S	37.774	6.05	46.47	6.90	15.19	433.59
								U-D	29.678	7.54	47.95	4.37	14.15	345.90
133	Adana	Feke	37.7455	35.8640	96.30	NA	NA	E-W	74.206	5.60	43.11	17.22	19.40	661.44
								N-S	77.882	6.88	44.02	10.91	21.21	517.13
								U-D	39.694	7.39	44.8	4.41	16.05	341.86
134	Adana	Feke	37.7443	35.8645	96.20	NA	NA	E-W	45.842	5.89	46.98	6.81	15.98	429.43
								N-S	68.712	7.32	42.35	12.43	21.72	555.86
								U-D	38.623	7.20	46	4.23	15.81	336.96

Station Code	City	District	Lat.	Long.	R_{rup}(km)	V_{S30} (m/s)	Site Class*	Comp.	PGA (cm/s^2)	PGV (cm/s)	Significant Duration (s)	Arias Intensity (cm/s)	Housner Intensity (cm)	Cumulative Absolute Velocity (cm/s)
2104	Diyarbakır	Ergani	38.2644	39.7590	99.70	NA	NA	E-W	88.006	13.13	46.3	17.75	66.55	694.58
								N-S	62.542	22.13	59.86	13.24	44.82	649.38
								U-D	42.838	8.70	72.97	6.72	28.38	500.67
2107	Diyarbakır	Çermik	38.1459	39.4838	74.70	NA	NA	E-W	112.283	16.51	43.8	28.72	66.62	858.16
								N-S	74.733	28.24	49.25	26.07	50.27	859.21
								U-D	44.231	7.88	56.72	8.13	32.05	489.21
2302	Elazığ	Maden	38.3923	39.6754	95.60	907	ZB	E-W	219.562	14.59	11.75	24.51	32.80	505.08
								N-S	197.116	14.05	13.23	20.65	24.32	491.13
								U-D	109.449	7.30	24.07	8.56	21.99	394.05
2308	Elazığ	Sivrice	38.4506	39.3102	68.90	450	ZC	E-W	163.792	29.35	37.31	35.35	98.63	808.03
								N-S	322.464	38.52	21.17	59.69	114.56	907.76
								U-D	400.053	11.53	10.14	39.50	32.90	600.52
2309	Elazığ	Keban	38.7991	38.7273	74.20	860	ZB	E-W	35.257	8.40	34.11	3.61	19.33	284.03
								N-S	36.858	6.67	40.39	4.19	14.58	326.56
								U-D	25.505	7.00	44.52	2.44	20.71	244.77
2310	Elazığ	Baskil	38.5727	38.8245	51.40	NA	NA	E-W	51.169	8.08	29.485	8.84	22.56	427.23
								N-S	60.480	14.85	22.055	10.56	33.19	443.03
								U-D	48.889	7.86	30.11	3.84	21.35	289.21
2703	Gaziantep	Şahinbey	37.0580	37.3500	51.40	758	ZC	E-W	160.131	16.67	53.08	120.01	49.54	1692.03
								N-S	150.388	13.32	52.5	114.58	43.44	1672.19
								U-D	80.294	8.02	52.08	31.18	29.32	882.75
2708	Gaziantep	İslahiye	37.0993	36.6484	4.00	523	ZC	E-W	1089.439	144.37	37.32	1154.32	488.24	3813.58
								N-S	812.734	126.86	39.91	963.64	361.96	3767.00
								U-D	977.012	55.92	20.57	439.64	149.64	2146.77
2711	Gaziantep	Yavuzeli	37.3174	37.5604	35.20	NA	NA	E-W	97.302	17.48	51.76	62.69	36.67	1251.38
								N-S	107.008	17.03	51.99	66.85	45.07	1270.04
								U-D	61.580	9.73	50.82	24.64	30.40	791.01
2712	Gaziantep	Nurdağı	37.1840	36.7328	1.00	NA	NA	E-W	602.742	110.46	33.96	744.30	332.38	3020.43
								N-S	555.436	83.02	36.7	628.04	197.28	2916.20
								U-D	343.814	26.90	38.09	237.04	97.04	1799.69

Station Code	City	District	Lat.	Long.	R_{rup}(km)	V_{S30} (m/s)	Site Class*	Comp.	PGA (cm/s^2)	PGV (cm/s)	Significant Duration (s)	Arias Intensity (cm/s)	Housner Intensity (cm)	Cumulative Absolute Velocity (cm/s)
2715	Gaziantep	İslahiye	36.8554	36.6856	9.80	NA	NA	E-W	340.021	55.52	46.99	132.07	82.08	1527.35
								N-S	457.193	36.99	45.29	110.24	66.06	1364.71
								U-D	76.072	13.61	49.12	14.02	44.61	533.71
2716	Gaziantep	İslahiye	36.8564	36.6883	10.00	NA	NA	E-W	228.890	55.57	48.72	232.49	147.00	2145.88
								N-S	255.463	60.13	49.91	266.12	142.58	2318.36
								U-D	164.684	17.00	50.73	100.29	54.05	1502.64
2717	Gaziantep	İslahiye	36.8555	36.6910	10.30	NA	NA	E-W	117.462	53.05	44.41	38.46	90.55	768.68
								N-S	138.367	32.96	49.92	29.18	58.59	703.65
								U-D	80.703	14.54	49.24	17.16	47.21	568.71
2718	Gaziantep	İslahiye	37.0078	36.6266	1.70	NA	NA	E-W	643.745	119.42	20.7	439.19	255.31	2229.45
								N-S	702.091	80.05	13.49	436.39	206.49	2125.73
								U-D	584.255	62.79	20.84	227.50	171.93	1564.41
3115	Hatay	Belen	36.5463	36.1646	19.10	424	ZC	E-W	211.134	50.82	37.52	172.62	153.67	1971.07
								N-S	274.824	42.12	29.65	321.62	166.45	2534.31
								U-D	214.353	20.58	30.79	114.75	78.51	1591.15
3116	Hatay	İskenderun	36.6162	36.2066	18.70	868	ZB	E-W	165.557	37.02	33.34	85.09	84.52	1216.03
								N-S	160.424	43.16	31.95	79.14	89.72	1227.89
								U-D	162.787	19.99	28.82	45.33	46.49	928.49
3123	Hatay	Antakya	36.2142	36.1597	14.40	470	ZC	E-W	594.043	101.98	17.68	754.41	401.08	3208.75
								N-S	655.302	188.44	13.58	935.11	579.51	3433.49
								U-D	868.061	52.67	14.09	487.14	215.76	2416.68
3124	Hatay	Antakya	36.2387	36.1722	11.70	283	ZD	E-W	637.793	101.28	18.86	776.20	391.19	3376.79
								N-S	572.431	113.10	21.39	622.95	444.00	3148.01
								U-D	577.756	42.70	17.08	317.40	144.70	1945.50
3125	Hatay	Antakya	36.2381	36.1326	14.60	448	ZC	E-W	1123.242	108.87	16.65	779.44	279.41	3057.58
								N-S	823.509	75.69	17.38	663.81	234.87	2956.75
								U-D	1136.121	65.49	9.74	823.35	144.35	2705.33
3126	Hatay	Antakya	36.2202	36.1375	15.40	350	ZD	E-W	1028.770	93.15	25.21	1134.59	274.03	4204.90
								N-S	1210.189	110.34	19.98	2096.96	380.30	5349.18
								U-D	1070.168	78.84	9.73	1288.69	207.89	3406.55

Station Code	City	District	Lat.	Long.	R_{rup}(km)	V_{S30} (m/s)	Site Class*	Comp.	PGA (cm/s^2)	PGV (cm/s)	Significant Duration (s)	Arias Intensity (cm/s)	Housner Intensity (cm)	Cumulative Absolute Velocity (cm/s)
3129	Hatay	Defne	36.1912	36.1343	17.90	447	ZC	E-W	1199.782	75.59	14.93	1829.59	286.96	4148.83
								N-S	1367.690	170.73	10.72	2501.64	545.19	4712.24
								U-D	826.167	43.85	10.22	705.19	165.12	2536.52
3131	Hatay	Antakya	36.1912	36.1633	16.20	567	ZC	E-W	339.689	44.24	8.98	164.62	222.30	1190.85
								N-S	349.297	51.49	9.06	127.52	168.36	974.83
								U-D	144.616	19.15	13.86	33.61	83.30	591.49
3132	Hatay	Antakya	36.2067	36.1716	14.40	377	ZC	E-W	514.114	53.85	17.58	439.50	221.47	2407.39
								N-S	515.074	67.69	13.52	372.47	294.44	2210.57
								U-D	353.840	34.28	13.64	193.77	154.21	1528.61
3133	Hatay	Reyhanlı	36.2432	36.5736	27.90	471	ZC	E-W	142.749	24.56	51.43	59.88	85.89	1215.67
								N-S	219.023	29.20	42.56	91.09	129.74	1387.28
								U-D	86.844	15.51	52.89	27.99	34.06	894.20
3134	Hatay	Dörtyol	36.8276	36.2049	28.20	374	ZC	E-W	203.742	41.95	45.6	127.59	108.57	1656.12
								N-S	245.988	40.58	45.58	143.25	136.27	1742.43
								U-D	140.627	19.87	43.68	57.74	46.07	1152.38
3135	Hatay	Arsuz	36.4089	35.8831	36.40	460	ZC	E-W	1367.456	66.09	22.78	688.44	232.35	2898.33
								N-S	741.091	51.94	23.33	558.60	183.14	2696.45
								U-D	589.311	37.45	25.25	244.53	95.77	1913.14
3136	Hatay	Altınözü	36.1159	36.2472	21.60	344	ZD	E-W	394.823	56.98	32.73	361.28	152.23	2619.67
								N-S	533.957	53.85	27.45	398.90	212.21	2604.43
								U-D	220.511	30.09	30.39	114.82	100.36	1469.17
3137	Hatay	Hassa	36.6929	36.4885	1.00	688	ZC	E-W	842.924	77.21	16.25	371.12	227.93	2183.54
								N-S	451.834	78.15	16.71	363.89	208.80	2239.28
								U-D	498.957	40.10	16.66	231.53	132.42	1760.51
3138	Hatay	Hassa	36.8026	36.5112	2.00	618	ZC	E-W	746.680	216.85	11.76	600.51	508.34	2281.25
								N-S	888.978	135.31	15.18	789.88	479.04	2596.21
								U-D	1068.095	83.22	4.99	325.55	331.92	1410.33
3139	Hatay	Kırıkhan	36.5838	36.4144	0.30	272	ZD	E-W	504.504	150.09	28.21	702.16	462.69	3216.46
								N-S	576.865	156.95	36.86	865.65	499.45	3675.59
								U-D	378.286	54.27	14.98	310.28	218.17	2078.78

Station Code	City	District	Lat.	Long.	R_{rup}(km)	V_{S30} (m/s)	Site Class*	Comp.	PGA (cm/s^2)	PGV (cm/s)	Significant Duration (s)	Arias Intensity (cm/s)	Housner Intensity (cm)	Cumulative Absolute Velocity (cm/s)
3140	Hatay	Samandağ	36.0816	35.9498	38.30	210	ZD	E-W	218.637	81.35	37.12	203.96	199.22	2117.51
								N-S	194.597	64.15	33.09	228.03	231.90	2174.74
								U-D	176.663	30.02	36.1	86.03	132.72	1381.62
3141	Hatay	Antakya	36.3726	36.2197	6.90	338	ZD	E-W	852.265	124.52	13.24	1535.79	409.43	4356.39
								N-S	944.346	83.15	16.02	1348.14	294.33	4356.39
								U-D	618.780	43.22	13.92	631.82	148.17	2808.10
3142	Hatay	Kırıkhan	36.4980	36.3661	0.40	539	ZC	E-W	746.416	76.48	12.01	606.18	208.40	2614.65
								N-S	647.205	87.84	11.65	568.60	214.84	2466.31
								U-D	503.662	30.59	12.97	224.09	74.89	1630.69
3143	Hatay	Hassa	36.8489	36.5571	0.40	445	ZC	E-W	351.295	106.44	26.4	252.12	253.16	1907.24
								N-S	381.318	129.53	23.32	273.54	272.79	1852.69
								U-D	411.649	28.96	18.2	171.59	107.58	1479.06
3144	Hatay	Hassa	36.7569	36.4857	2.10	535	ZC	E-W	763.724	138.98	39.83	386.29	250.32	2532.92
								N-S	611.555	138.07	31.9	356.72	271.92	2157.42
								U-D	452.311	80.17	15.92	138.31	235.81	1249.10
3145	Hatay	Kırıkhan	36.6454	36.4064	3.70	533	ZC	E-W	696.562	157.69	11.14	657.04	398.21	2350.18
								N-S	599.876	116.51	13.68	386.67	235.53	2053.54
								U-D	660.538	64.79	10.59	315.71	233.36	1713.35
3146	Hatay	Belen	36.4908	36.2270	11.50	NA	NA	E-W	346.000	54.23	17.68	330.91	117.21	1780.37
								N-S	481.686	39.20	15.83	494.37	124.40	2140.70
								U-D	340.118	19.07	18.91	205.62	73.36	1439.78
3147	Hatay	Yayladağı	35.9024	36.0644	48.80	NA	NA	E-W	47.500	27.15	34.59	8.28	42.59	439.66
								N-S	56.468	14.90	55.08	7.33	37.06	427.90
								U-D	29.130	8.12	43.22	4.15	28.59	324.59
4404	Malatya	Pütürge	38.1959	38.8739	22.30	1380	ZB	E-W	136.236	15.11	21.99	19.53	39.40	561.83
								N-S	135.323	21.21	21.29	20.68	42.58	580.56
								U-D	95.803	10.62	29.06	9.47	34.42	425.68
4405	Malatya	Hekimhan	38.8107	37.9396	94.50	579	ZC	E-W	126.383	15.88	21.91	19.27	26.12	537.06
								N-S	90.736	8.27	26.79	13.63	24.49	498.48
								U-D	77.207	7.55	26.47	9.81	26.90	424.74

Station Code	City	District	Lat.	Long.	R_{rup}(km)	V_{S30} (m/s)	Site Class*	Comp.	PGA (cm/s^2)	PGV (cm/s)	Significant Duration (s)	Arias Intensity (cm/s)	Housner Intensity (cm)	Cumulative Absolute Velocity (cm/s)
4406	Malatya	Akçadağ	38.3439	37.9738	47.50	815	ZB	E-W	131.322	29.17	40.21	33.07	75.67	827.57
								N-S	108.849	14.16	46.01	24.16	36.53	757.00
								U-D	49.838	12.31	45.8	11.43	35.80	528.86
4407	Malatya	Arguvan	38.7807	38.2641	78.40	735	ZC	E-W	33.083	8.41	57.45	6.63	32.83	452.77
								N-S	43.351	13.41	52.11	8.31	34.17	494.37
								U-D	19.328	7.06	53.29	2.68	21.35	284.76
4408	Malatya	Doğanşehir	38.0962	37.8873	27.00	654	ZC	E-W	137.188	35.73	25.96	43.45	74.74	834.86
								N-S	100.331	24.95	28.43	23.98	46.41	665.23
								U-D	96.811	22.86	26.66	23.03	64.05	632.99
4409	Malatya	Darende	38.5606	37.4908	88.90	NA	NA	E-W	28.488	10.01	55.96	3.54	15.39	328.41
								N-S	38.057	7.34	51.24	4.71	19.69	365.29
								U-D	27.983	6.97	52.32	2.97	18.09	293.85
4412	Malatya	Yazıhan	38.5969	38.1839	63.50	NA	NA	E-W	68.867	48.20	50.09	45.56	71.11	1141.01
								N-S	63.657	27.18	45.2	31.35	68.41	970.82
								U-D	55.550	27.27	53.73	25.02	51.08	893.72
4611	Kahramanmaraş	Çağlayancerit	37.7472	37.2843	18.50	731	ZC	E-W	320.401	40.08	43.62	267.64	118.32	2349.00
								N-S	349.470	42.52	42.58	281.65	117.18	2371.06
								U-D	173.891	15.69	45.71	83.16	50.23	1331.88
4612	Kahramanmaraş	Göksun	38.0240	36.4819	79.70	246	ZD	E-W	122.210	14.90	55.12	127.63	65.19	1999.99
								N-S	140.979	20.54	56.74	102.01	59.11	1801.96
								U-D	54.192	5.24	57.98	20.14	18.80	808.91
4613	Kahramanmaraş	Andırın	37.5701	36.3574	48.80	NA	NA	E-W	153.576	10.87	40.18	63.02	28.89	1183.87
								N-S	146.858	15.80	41.11	50.95	27.48	1079.53
								U-D	75.032	14.33	42.27	21.59	17.23	710.82
4615	Kahramanmaraş	Pazarcık	37.3868	37.1380	10.30	484	ZC	E-W	581.134	131.96	47.1	605.26	314.76	3263.48
								N-S	583.931	152.43	46.65	584.93	247.03	3188.66
								U-D	664.518	77.88	35.66	305.41	159.44	2106.71
4616	Kahramanmaraş	Türkoğlu	37.3755	36.8384	2.30	390	ZC	E-W	505.824	87.46	41.03	387.30	202.84	2544.91
								N-S	615.281	97.90	41.8	658.17	224.19	3200.42
								U-D	398.751	25.86	39	226.83	72.11	1881.56

Station Code	City	District	Lat.	Long.	R_{rup}(km)	V_{S30} (m/s)	Site Class*	Comp.	PGA (cm/s^2)	PGV (cm/s)	Significant Duration (s)	Arias Intensity (cm/s)	Housner Intensity (cm)	Cumulative Absolute Velocity (cm/s)
4617	Kahramanmaraş	Onikişubat	37.5855	36.8303	22.20	574	ZC	E-W	114.831	28.24	44.49	57.19	72.96	1136.16
								N-S	145.430	29.44	44.33	74.46	83.33	1221.48
								U-D	110.736	20.70	45.61	47.88	48.26	1039.63
4620	Kahramanmaraş	Onikişubat	37.5857	36.8985	19.30	484	ZC	E-W	320.589	38.65	44.77	262.99	84.29	2259.75
								N-S	300.302	32.80	42.41	233.33	77.20	2070.83
								U-D	185.071	15.93	46.18	116.64	51.40	1552.32
4624	Kahramanmaraş	Onikişubat	37.5361	36.9177	13.70	280	ZD	E-W	319.801	62.40	45.84	437.35	201.39	2960.10
								N-S	357.389	60.48	45.96	389.34	199.05	2739.93
								U-D	161.694	35.76	43.39	112.44	82.91	1522.63
4625	Kahramanmaraş	Dulkadiroğlu	37.5387	36.9819	11.10	346	ZD	E-W	484.376	67.12	41.52	468.82	179.44	2815.40
								N-S	448.106	79.80	38.15	429.77	225.64	2702.33
								U-D	367.233	28.98	31.82	233.97	93.09	1989.10
4628	Kahramanmaraş	Afşin	38.2412	36.9228	81.90	337	ZD	E-W	82.565	11.91	58.19	56.67	28.65	1334.30
								N-S	91.116	9.74	55.09	44.83	22.60	1176.45
								U-D	55.744	4.10	57.43	10.22	11.99	548.17
6303	Şanlıurfa	Siverek	37.7524	39.3291	74.70	986	ZB	E-W	114.461	21.71	35.04	20.09	67.92	658.33
								N-S	117.418	17.11	40.51	17.22	56.21	610.16
								U-D	38.915	10.44	67.83	8.48	26.27	561.84
6304	Şanlıurfa	Bozova	37.3651	38.5132	70.70	376	ZC	E-W	237.995	16.55	46.29	181.45	54.76	2187.95
								N-S	210.759	21.30	44.07	152.30	63.06	1962.59
								U-D	89.436	11.23	53.65	34.88	23.26	1018.96
8002	Osmaniye	Bahçe	37.1916	36.5620	15.20	430	ZC	E-W	202.594	41.44	41.48	126.09	79.36	1558.71
								N-S	242.513	45.00	36.08	241.39	142.78	2089.51
								U-D	335.052	18.41	33.78	167.12	61.90	1669.63
8003	Osmaniye	Osmaniye Merkez	37.0842	36.2694	34.20	350	ZD	E-W	185.872	28.60	39.62	115.09	102.30	1587.76
								N-S	141.600	31.33	38.88	91.13	113.60	1363.10
								U-D	139.941	19.59	41.22	63.66	65.90	1159.75
8004	Osmaniye	Kadirli	37.3799	36.0976	61.20	426	ZC	E-W	178.978	22.00	44.16	96.90	70.54	1483.75
								N-S	168.388	19.05	41.88	80.42	58.55	1316.69
								U-D	71.815	12.04	51.62	18.86	36.19	718.60
NAR	Kahramanmaraş	Pazarcık	37.3919	37.1574	10.70	NA	NA	E-W	613.878	104.40	40.77	366.97	223.00	2494.04
								N-S	765.851	90.45	38.49	393.03	212.27	2484.29
								U-D	482.223	46.27	33.81	230.63	108.15	1868.44

*Site classes are given according to the site classification of the 2019 edition of earthquake code in Turkey (TBEC, 2019).

Table 4.2. Information on Recorded Strong Ground Motions of Elbistan earthquake for stations within 100 km rupture distance (unknown V_{S30}/Site Class values are shown with NA)

Station Code	City	District	Lat.	Long.	R_{rup} (km)	V_{S30} (m/s)	Site Class*	Comp.	PGA (cm/s^2)	PGV (cm/s)	Significant Duration (s)	Arias Intensity (cm/s)	Housner Intensity (cm)	Cumulative Absolute Velocity (cm/s)
127	Adana	Feke	37.8162	35.9204	73.70	583	ZC	E-W	62.75	13.98	37.36	11.09	25.76	476.64
								N-S	56.07	16.16	39.62	8.04	21.29	406.54
								U-D	38.25	14.97	35.05	4.13	15.77	289.93
129	Adana	Tufanbeyli	38.2592	36.2109	55.40	965	ZB	E-W	172.34	15.85	23.97	33.59	24.02	700.45
								N-S	154.48	19.38	25.61	37.60	27.95	747.15
								U-D	85.49	14.49	28.42	13.35	22.38	455.09
131	Adana	Saimbeyli	37.8566	36.1153	56.00	NA	NA	E-W	331.27	27.35	16.16	91.60	26.80	1023.91
								N-S	397.23	27.44	14.21	120.83	31.20	1111.82
								U-D	83.37	18.65	23.30	11.38	26.20	415.91
132	Adana	Saimbeyli	37.8559	36.1149	56.10	NA	NA	E-W	59.45	14.02	31.21	5.12	17.08	305.73
								N-S	65.34	21.25	25.79	6.30	20.85	304.53
								U-D	53.67	17.42	26.92	6.45	26.08	318.86
133	Adana	Feke	37.7455	35.8640	80.80	NA	NA	E-W	80.24	18.23	33.42	13.07	23.24	491.70
								N-S	47.33	14.42	42.44	6.34	23.55	359.03
								U-D	36.93	13.14	42.31	3.77	16.75	282.31
134	Adana	Feke	37.7443	35.8645	80.80	NA	NA	E-W	46.53	18.86	38.42	6.13	22.36	343.00
								N-S	52.13	13.20	36.89	8.01	25.85	395.68
								U-D	35.49	13.83	41.51	3.49	17.00	271.08
138	Adana	Kozan	37.7049	35.7234	93.90	NA	NA	E-W	22.89	12.54	37.55	1.96	14.17	205.84
								N-S	25.02	12.56	40.50	1.61	13.98	185.09
								U-D	18.85	10.06	47.83	1.60	14.27	195.23
205	Adıyaman	Kahta	37.7918	38.6160	90.60	660	ZC	E-W	54.65	22.13	40.82	14.53	50.06	613.56
								N-S	44.88	16.00	47.30	12.16	48.73	579.42
								U-D	32.93	10.75	56.32	7.92	28.62	480.97
213	Adıyaman	Tut	37.7967	37.9296	39.90	NA	NA	E-W	126.66	24.00	29.76	79.91	102.01	1227.56
								N-S	121.24	26.68	30.35	73.64	83.89	1189.88
								U-D	71.36	9.93	31.81	18.33	30.87	594.91
3802	Kayseri	Sarız	38.4781	36.5036	59.00	305	ZD	E-W	220.92	27.65	47.84	111.97	138.82	1610.08
								N-S	196.54	25.73	44.60	122.52	113.17	1647.43
								U-D	121.64	12.59	57.00	44.66	63.26	1052.04

Station Code	City	District	Lat.	Long.	R_{rup} (km)	V_{S30} (m/s)	Site Class*	Comp.	PGA (cm/s^2)	PGV (cm/s)	Significant Duration (s)	Arias Intensity (cm/s)	Housner Intensity (cm)	Cumulative Absolute Velocity (cm/s)
3804	Kayseri	Pınarbaşı	38.7227	36.3779	88.30	637	ZC	E-W	37.97	6.62	34.96	3.52	19.88	252.56
								N-S	34.55	8.54	44.31	3.02	17.06	251.90
								U-D	27.89	4.81	45.80	2.13	13.48	220.64
4405	Malatya	Hekimhan	38.8107	37.9396	85.30	579	ZC	E-W	156.98	14.62	20.48	22.13	33.61	549.93
								N-S	152.09	7.96	20.30	22.85	34.37	571.37
								U-D	119.33	8.55	20.02	12.49	25.61	418.75
4406	Malatya	Akçadağ	38.3439	37.9738	41.00	815	ZB	E-W	410.95	36.95	17.42	287.52	97.76	1784.12
								N-S	472.03	22.36	18.37	326.12	94.34	1955.80
								U-D	315.16	19.11	16.98	144.70	62.52	1274.76
4409	Malatya	Darende	38.5606	37.4908	55.00	NA	NA	E-W	76.99	18.56	31.17	15.15	45.44	510.97
								N-S	72.04	9.19	27.40	15.17	33.30	511.09
								U-D	53.53	6.80	31.56	7.89	25.80	386.26
4410	Malatya	Kuluncak	38.8668	37.6790	87.70	NA	NA	E-W	127.27	17.64	25.61	25.78	48.18	659.64
								N-S	112.08	10.03	26.57	19.04	43.18	582.30
								U-D	54.04	5.36	31.38	7.03	24.49	382.82
4412	Malatya	Yazıhan	38.5969	38.1839	74.20	NA	NA	E-W	126.37	28.65	35.05	45.11	91.57	979.39
								N-S	158.97	39.50	35.32	50.21	101.56	1002.06
								U-D	79.91	29.18	52.34	37.08	63.22	1000.96
4611	Kahramanmaraş	Çağlayancerit	37.7472	37.2843	32.30	731	ZC	E-W	138.66	38.36	32.77	68.55	78.22	1080.46
								N-S	194.41	14.19	35.09	56.78	49.96	996.46
								U-D	69.66	11.35	35.43	14.90	30.36	532.72
4612	Kahramanmaraş	Göksun	38.0240	36.4819	22.70	246	ZD	E-W	523.19	75.57	25.33	317.38	314.81	1919.10
								N-S	635.48	174.05	20.01	417.35	410.67	2070.85
								U-D	367.81	55.89	9.99	89.83	129.34	875.16
4614	Kahramanmaraş	Pazarcık	37.4851	37.2978	61.30	541	ZC	E-W	203.92	34.77	33.63	51.91	33.49	952.45
								N-S	160.92	13.38	32.39	63.00	25.68	1081.29
								U-D	89.17	5.48	34.67	14.20	17.03	508.92
4615	Kahramanmaraş	Pazarcık	37.3868	37.1380	70.20	484	ZC	E-W	73.58	30.44	39.73	13.88	35.02	549.36
								N-S	44.44	10.99	39.04	8.73	20.99	426.76
								U-D	41.63	6.64	42.74	3.95	14.98	293.52

Station Code	City	District	Lat.	Long.	R_{rup} (km)	V_{S30} (m/s)	Site Class*	Comp.	PGA (cm/s^2)	PGV (cm/s)	Significant Duration (s)	Arias Intensity (cm/s)	Housner Intensity (cm)	Cumulative Absolute Velocity (cm/s)
4616	Kahramanmaraş	Türkoğlu	37.3755	36.8384	67.80	390	ZC	E-W	53.42	14.71	35.45	9.60	16.94	432.47
								N-S	57.55	10.69	37.61	11.35	16.67	479.10
								U-D	28.04	5.44	39.97	3.09	13.16	261.15
4617	Kahramanmaraş	Onikişubat	37.5855	36.8303	44.60	574	ZC	E-W	82.56	28.47	37.21	27.30	77.74	728.53
								N-S	55.90	23.46	39.76	19.15	60.60	642.67
								U-D	54.76	13.54	44.86	12.24	53.54	540.45
4620	Kahramanmaraş	Onikişubat	37.5857	36.8985	45.40	484	ZC	E-W	81.18	25.19	45.54	19.64	59.58	651.81
								N-S	66.83	21.99	37.52	15.83	50.54	583.58
								U-D	57.04	13.62	40.51	8.89	44.94	446.19
4624	Kahramanmaraş	Onikişubat	37.5361	36.9177	51.10	280	ZD	E-W	79.83	19.24	45.46	25.12	52.11	765.68
								N-S	65.03	18.78	42.96	26.06	65.10	770.11
								U-D	38.60	9.04	44.38	6.69	30.09	391.69
5807	Sivas	Gürün	38.7269	37.2475	76.10	445	ZC	E-W	71.85	17.86	33.78	17.60	47.48	571.91
								N-S	90.60	10.61	32.94	23.84	33.54	668.98
								U-D	41.84	7.43	39.05	9.11	29.98	444.45
8002	Osmaniye	Bahçe	37.1916	36.5620	89.00	430	ZC	E-W	45.52	18.16	36.32	6.51	23.88	387.75
								N-S	65.88	7.74	32.27	11.68	29.08	474.35
								U-D	28.81	6.81	47.19	4.02	16.28	317.22
NAR	Kahramanmaraş	Pazarcık	37.3919	37.1574	69.90	NA	NA	E-W	109.90	27.50	32.16	11.75	21.97	404.07
								N-S	126.47	8.65	28.54	9.79	17.30	362.86
								U-D	82.38	4.76	29.04	5.45	9.99	264.15

*Site classes are given according to the site classification of the 2019 edition of earthquake code in Turkey (TBEC, 2019).

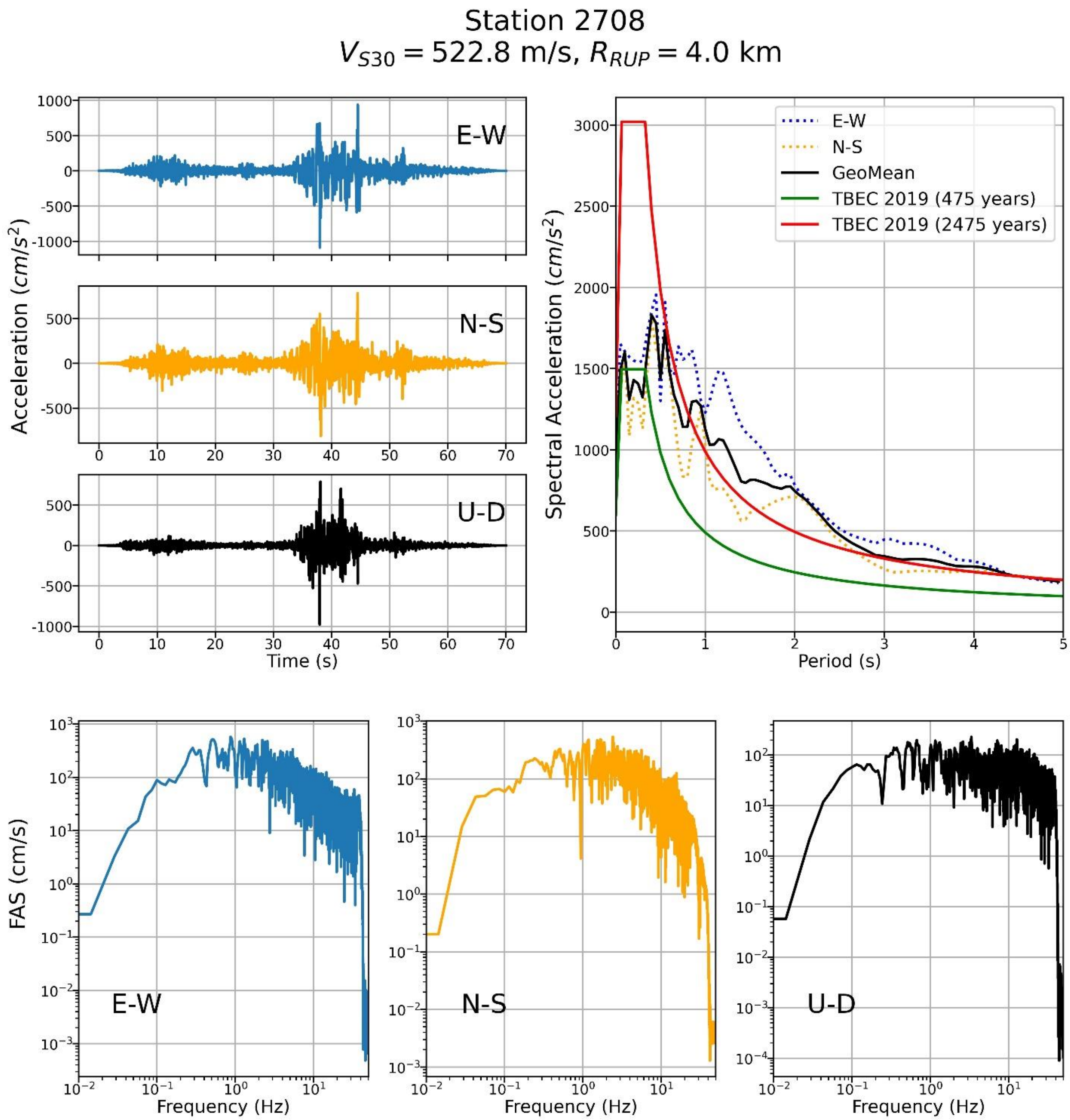

Figure 4.8. Recorded three-component ground accelerations, corresponding Fourier amplitude spectra (FAS) and response spectra (with 5% damping) in comparison with the most recent building code (TBEC, 2019) at selected station 2708 due to Pazarcik (Mw=7.7) event

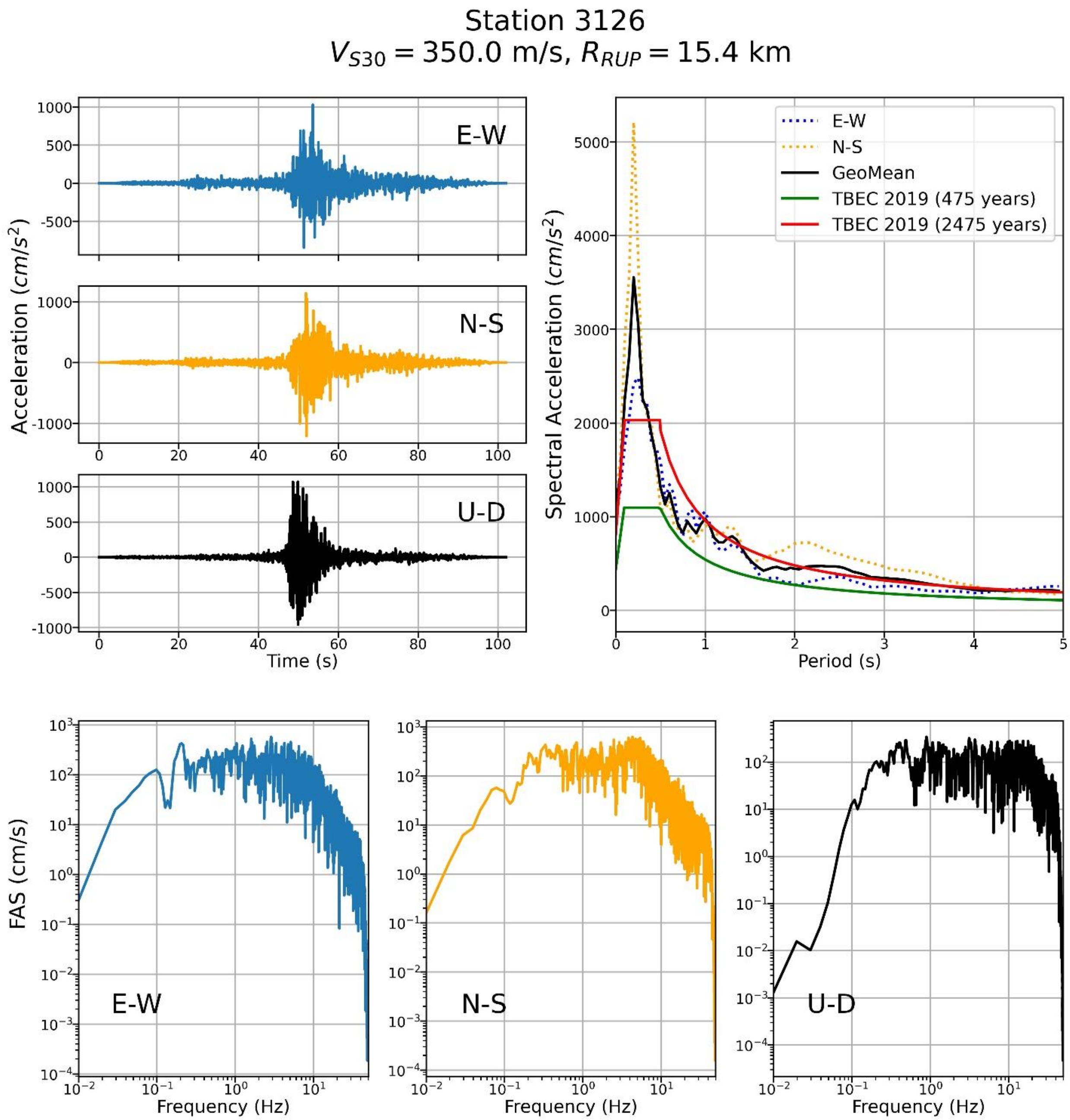

Figure 4.9. Recorded three-component ground accelerations, corresponding Fourier amplitude spectra (FAS) and response spectra (with 5% damping) in comparison with the most recent building code (TBEC, 2019) at selected station 3126 due to Pazarcik (Mw=7.7) event

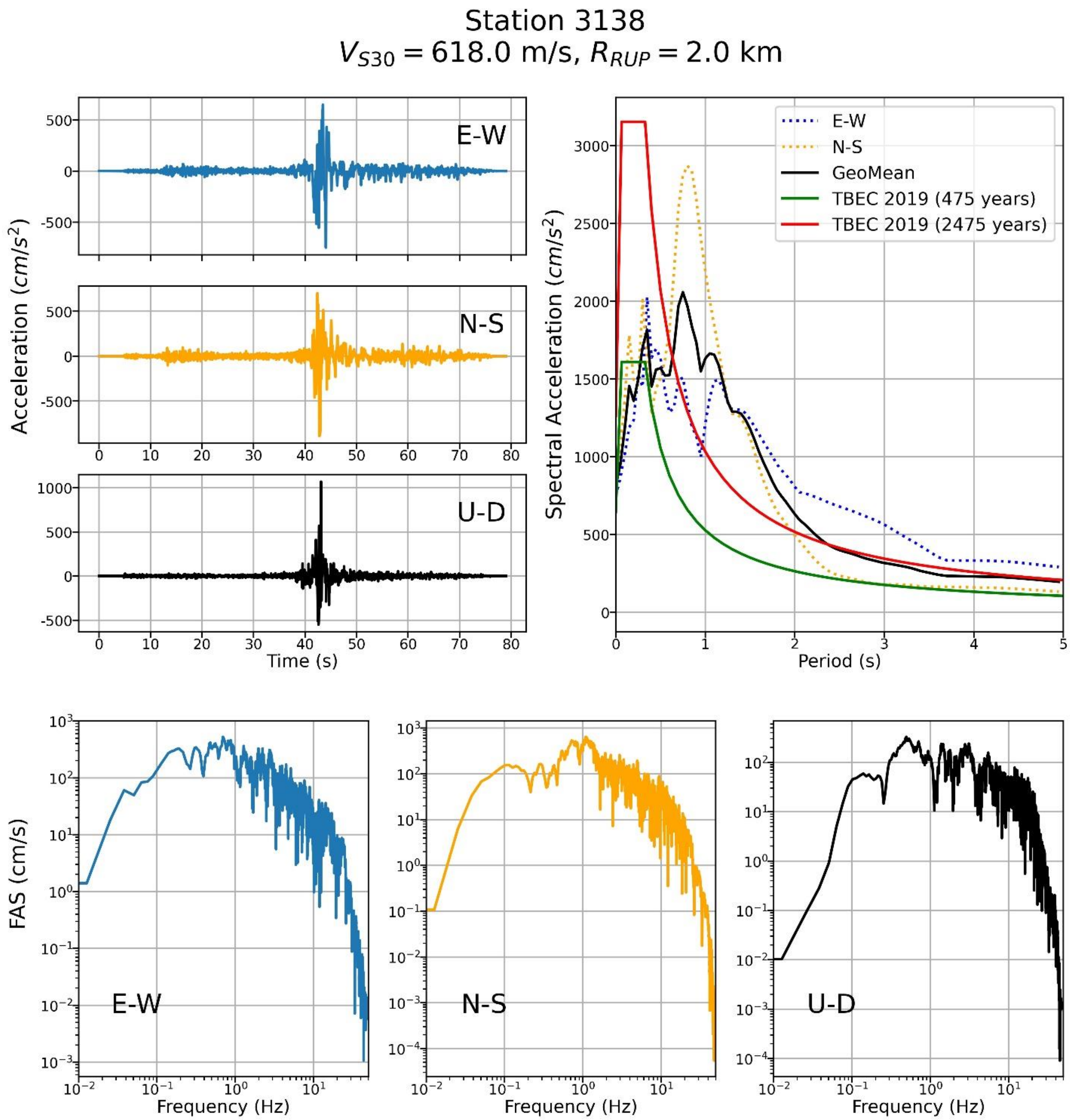

Figure 4.10. Recorded three-component ground accelerations, corresponding Fourier amplitude spectra (FAS) and response spectra (with 5% damping) in comparison with the most recent building code (TBEC, 2019) at selected station 3138 due to Pazarcik (Mw=7.7) event

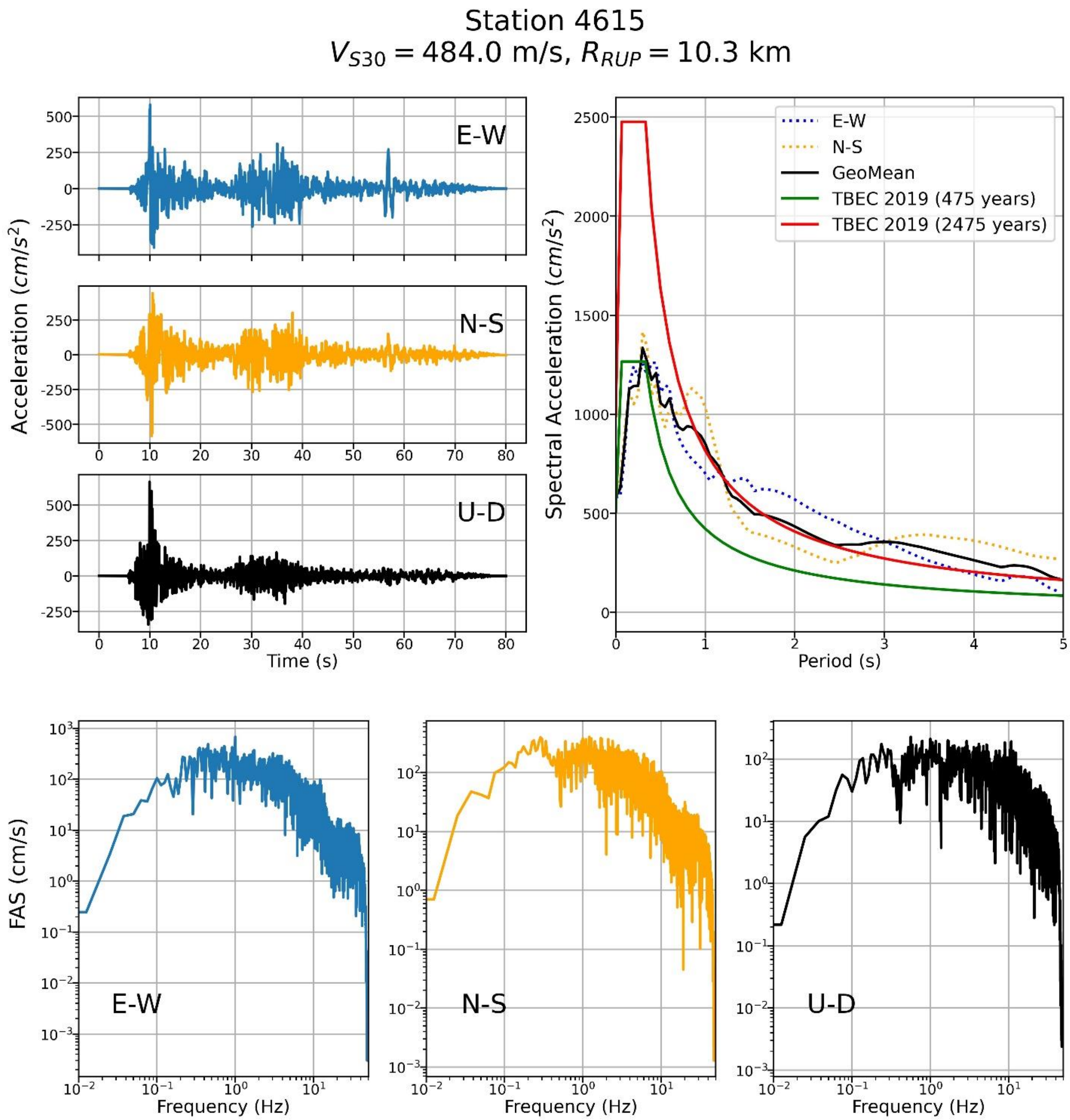

Figure 4.11. Recorded three-component ground accelerations, corresponding Fourier amplitude spectra (FAS) and response spectra (with 5% damping) in comparison with the most recent building code (TBEC, 2019) at selected station 4615 due to Pazarcik (Mw=7.7) event

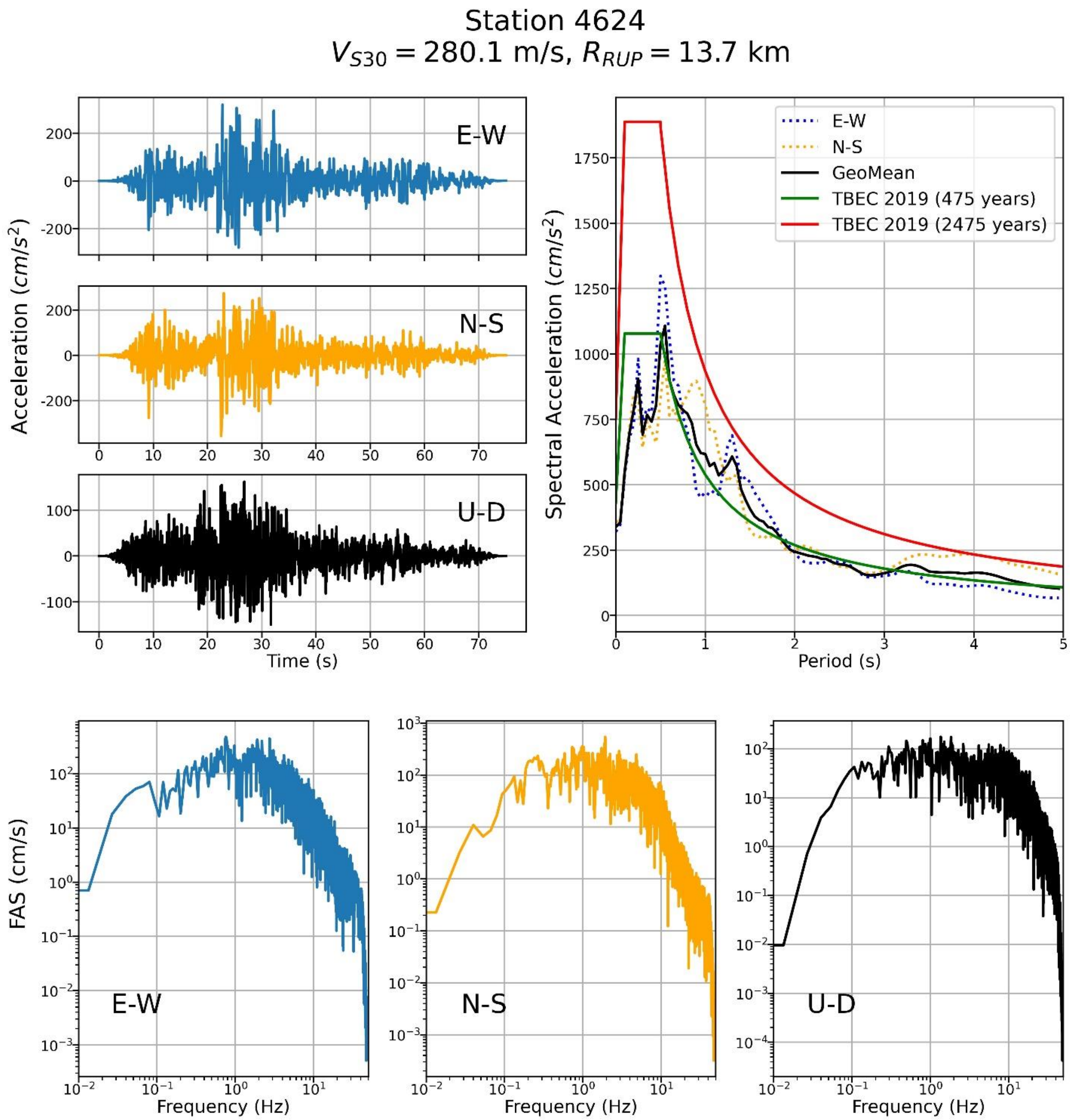

Figure 4.12. Recorded three-component ground accelerations, corresponding Fourier amplitude spectra (FAS) and response spectra (with 5% damping) in comparison with the most recent building code (TBEC, 2019) at selected station 4624 due to Pazarcik (Mw=7.7) event

Station 2708 is located in Islahiye, Gaziantep, on a site with NEHRP site class C (site class ZC of TBEC, 2019) and at a rupture distance of 4 km. We note that multiple wave packets were observed in the accelerogram. Both the FAS and response spectra were computed based on the entire time series, including all wave packets provided by AFAD. The maximum horizontal PGA is recorded in the EW direction as 1089 cm/s^2, while the vertical PGA value was recorded as 977 cm/s^2. The broadband nature of the response spectrum is attributed to the multiple wave packets observed in this large event. Response spectra from both horizontal components show peaks in the short period range. Despite being located on stiff soil conditions; the response spectra of the EW component shows clear amplifications also in the longer periods with a particular peak around 1.2 seconds. The geometric mean of two horizontal response spectra exceeds the design spectrum corresponding to a return period of 475 years at almost all periods. The same geometric mean exceeds the design spectrum for a return period of 2475 years for periods longer than 0.7 seconds. We note that the most destruction was concentrated in this region based on the first observations in the field.

Station 3126 is located in Antakya, on a site with NEHRP site class D (site class ZD of TBEC, 2019) with a rupture distance of 15.4 km. The maximum horizontal PGA is recorded in the NS direction as 1210 cm/s^2. The vertical PGA value is 1070 cm/s^2. We observe that the acceleration recorded in the vertical direction are similar to those recorded in the horizontal direction in terms of frequency and amplitude content. The response spectra of both EW and NS components indicate amplifications around 0.3 seconds and both exceed the design spectrum for a return period of 475 years. The geometric mean is above the design spectrum for a return period of 2475 years for periods less than 0.4 seconds and below for longer periods.

Station 3138 is located in Hassa, Hatay on a site with NEHRP site class C (site class ZC of TBEC, 2019) with a rupture distance of 2 km. The acceleration records suggest potential directivity effects. When velocities are investigated, this record indicates forward directivity effects characterized by short-duration and high-amplitude, two-sided long-period velocity pulses. The geometric mean of horizontal response spectra indicates broadband period content and exceeds the design spectrum for a return period of 475 years for periods longer than 0.4 seconds.

Station 4615 is located in Pazarcik on a site with NEHRP site class C (site class ZC of TBEC, 2019) at a rupture distance of 10.3 km. This record also displays broadband response spectra, possibly due to the multiple wave packets. The maximum PGA value is recorded in the vertical component as 664 cm/s^2. The geometric mean spectrum is observed to exceed the 475-year design spectrum at periods larger than 0.5 s, and it is shown to be similar to the 2475-year design spectrum at periods larger than 1 s.

Station 4624, located in Onikisubat, Kahramanmaraş on a NEHRP site class D (site class ZD of TBEC, 2019) at a rupture distance of 13.7 km. The maximum horizontal PGA of 357 cm/s^2, which is relatively lower than the values at other stations. However, the geometric mean of the horizontal response spectra still exceeds the design spectrum for a return period of 475 years at periods longer than 0.7 seconds. The broadband content of the response spectra is consistent with the multiple wave packets observed in the accelerogram.

4.3.1. MMI Distribution

Assessing seismic intensity measures after an earthquake is of great importance in identifying the effects of varying ground shaking over an area. One of the most common intensity measures for a rapid evaluation of seismic effects is macroseismic intensity distributions. Intensity levels can be assigned in the field, estimated via online surveys based on human responses, or can be computed via ground motion to intensity conversion equations (GMICEs). GMICEs mainly employ peak strong ground motion parameters such as PGA and PGV.

Within the scope of this report, Modified Mercalli Intensity (MMI) maps are used for the Pazarcik earthquake (7.7 Mw) and Elbistan earthquake (7.5 Mw) to identify the affected locations. Since the majority of the building stock in the mostly damaged regions is composed of rigid, low-to-mid-rise buildings, PGA could be a better identifier for macroseismic intensity distributions rather than PGV, which better correlates with the seismic behavior of ductile reinforced concrete structures (Erberik, 2008a; Erberik, 2008b). In this report, PGA-based ground motion to intensity conversion equations of Bilal and Askan (2014) and Albayrak et al. (2023) are employed. These GMICEs are both derived from local data compiled after past events in Türkiye. They both rely on geometric means of horizontal PGA values (in cm/s^2) from 244 strong ground motion stations for the defined earthquakes. The equations of Bilal and Askan (2014) and Albayrak et al. (2023) are as follows:

$$MMI = 0.132 + 3.884 \log PGA \tag{4.1}$$

$$MMI = 1.290 + 3.766 \log PGA \tag{4.2}$$

MMI levels can be related to anticipated damage levels. These damage levels are approximately moderate damage, moderate-to-severe damage and severe damage or total collapse as MMI levels of VI-VIII, VIII-X, and X-XII, respectively. Figure 4.13 shows the station-based MMI levels for Pazarcik Earthquake. Locations in the close vicinity of the epicenter exhibit MMI levels between X and XII. Figure 4.14 shows the station-based MMI levels for Elbistan earthquake. Locations in the close vicinity of the epicenter exhibit MMI levels between VIII and X.

It should be underlined that the Pazarcik earthquake had severe seismic effects not only around the epicenter but also along the surface rupture. In contrast, the MMI levels for Elbistan earthquake imply moderate-to-severe damage around the epicenter. It is important to note that MMI levels presented here express the effects of these two events independently. However, the occurrence of two large consecutive earthquakes in a relatively short time undoubtedly increased the damage levels in the structures located in the region. Finally, for regions with mid- and high-rise flexible reinforced concrete structures, PGV-based ground motion to intensity conversion equations should also be examined (Albayrak et al. 2023; Erberik, 2008a; Erberik, 2008b).

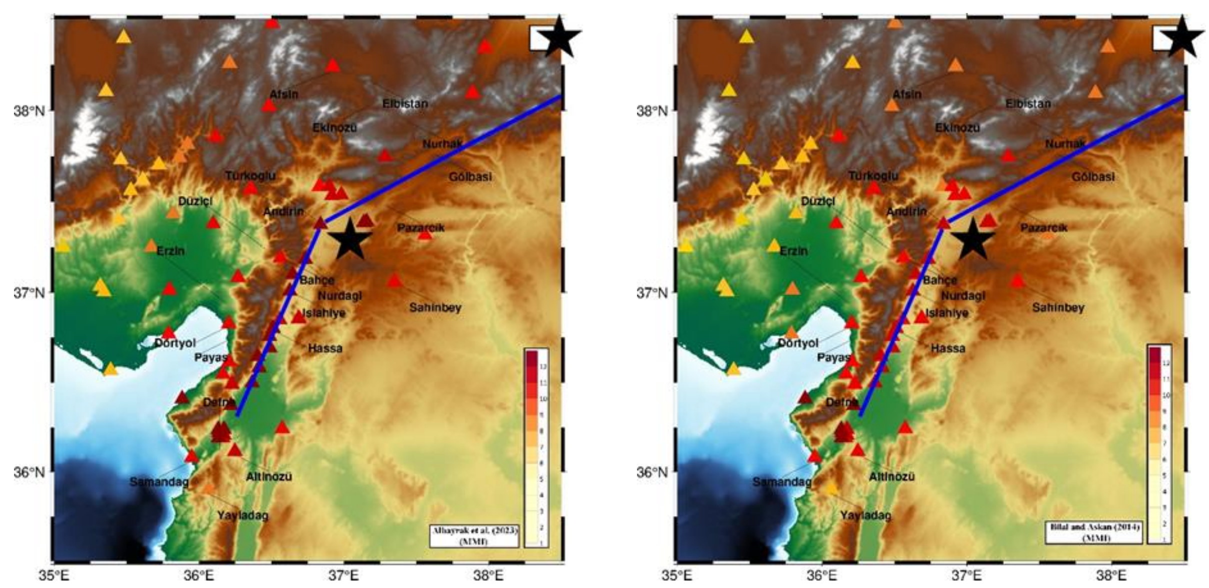

(a) (b)

Figure 4.13. Station based MMI levels for Pazarcik earthquake using recorded PGA values for (a) Equation 4.1 and (b) Equation 4.2.

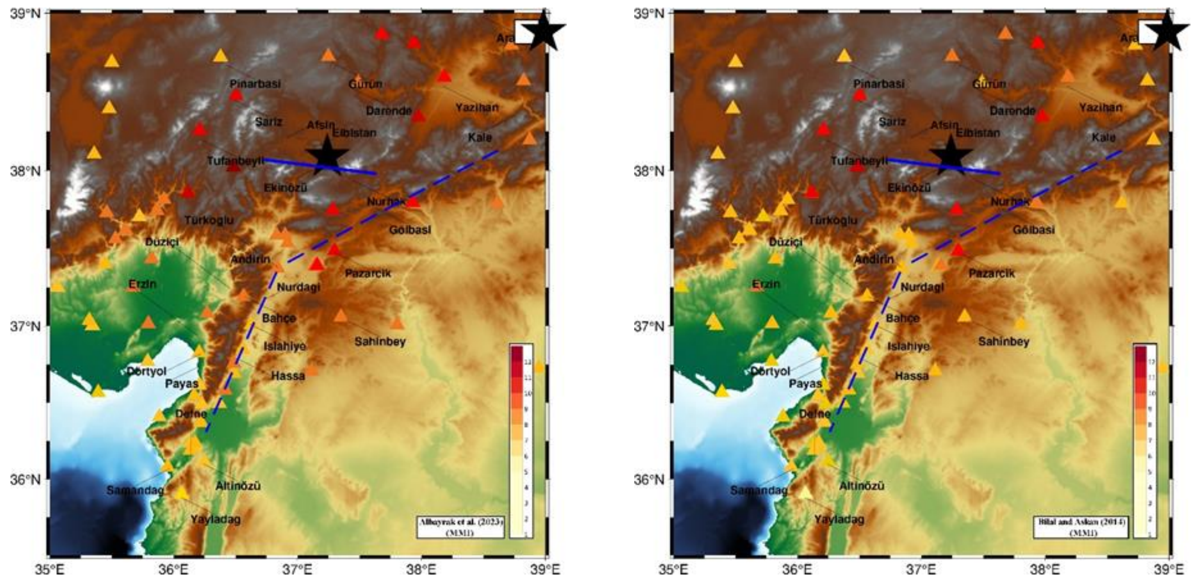

(a) (b)

Figure 4.14. Station based MMI levels for Elbistan earthquake using recorded PGA values for (a) Equation 4.1 and (b) Equation 4.2.

4.4. Spatial Distribution of Peak and Spectral Accelerations

The spatial distribution of peak and spectral accelerations for the Pazarcik and Elbistan earthquakes is shown in Figures 4.15 and 4.16, respectively. Upon investigation of Figure 4.15, it becomes apparent that the highest PGA values are recorded in Antakya. In addition, very high PGA values between 500-1000 cm/s^2 are observed generally in the North-South direction, covering the provinces of Kahramanmaraş, Gaziantep, Osmaniye, Kilis and Hatay. The distribution of PGV and short-period spectral acceleration (at T=0.2 s) values are more homogeneous compared to the PGA, with very high intensities at all stations close to the rupture. Finally, the higher long-period spectral acceleration values (at T=1 s) observed in Antakya indicate potential forward directivity effects. As for the Elbistan earthquake (M_w=7.5), it is not as densely-recorded as the Pazarcik (M_w=7.7) event. As the rupture is located to the north of the first event (Figure 4.16), the effects of this event are felt more noticeably in the northern provinces, in addition to Kahramanmaraş, such as Adıyaman, Malatya and Kayseri. The highest ground motion intensities are generally observed in Kahramanmaraş.

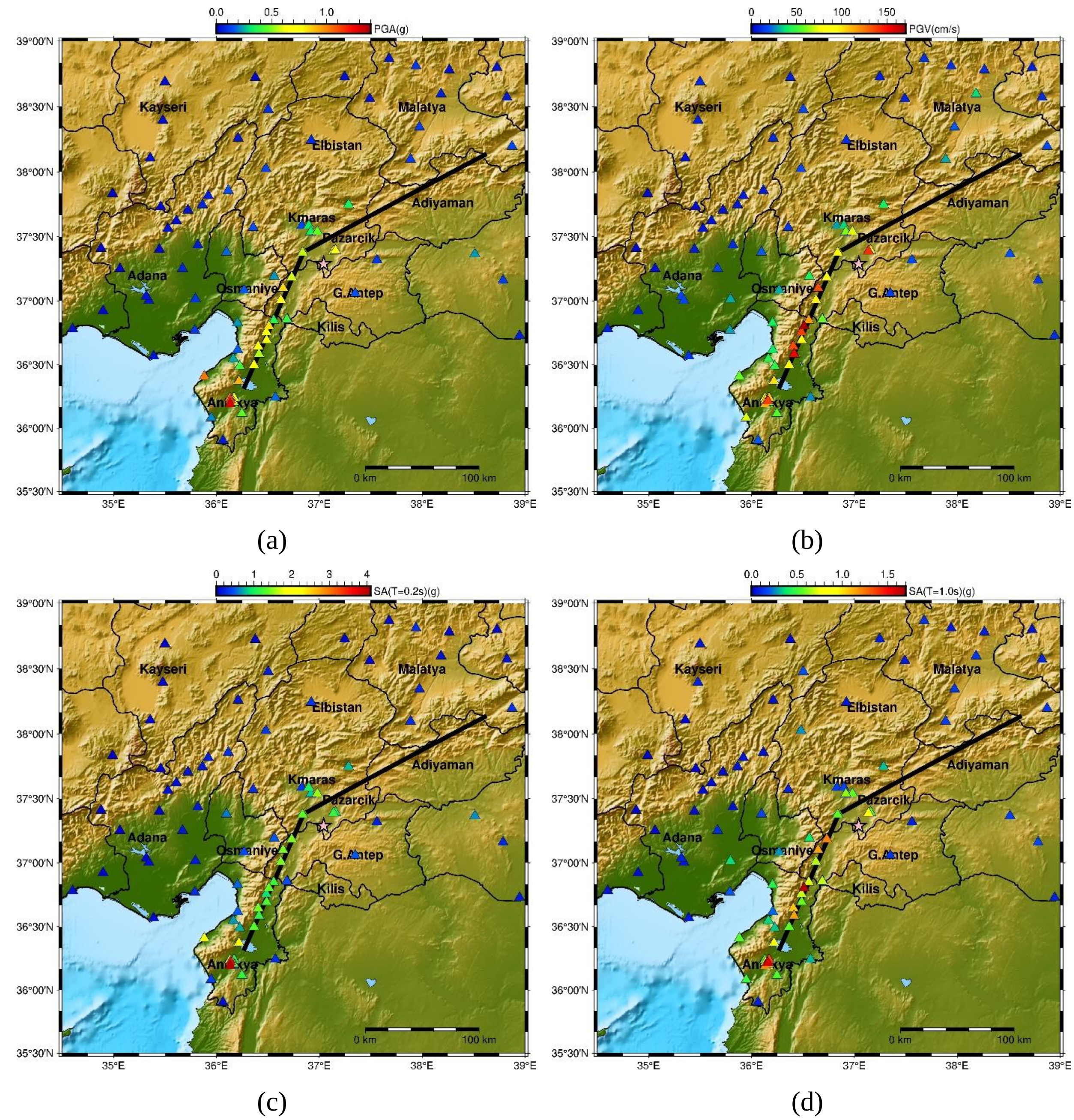

Figure 4.15. Spatial distribution of intensity measure of Pazarcik earthquake (a) PGA, (b) PGV, (c) T=0.2 s PSA and (d) T=1.0 s PSA

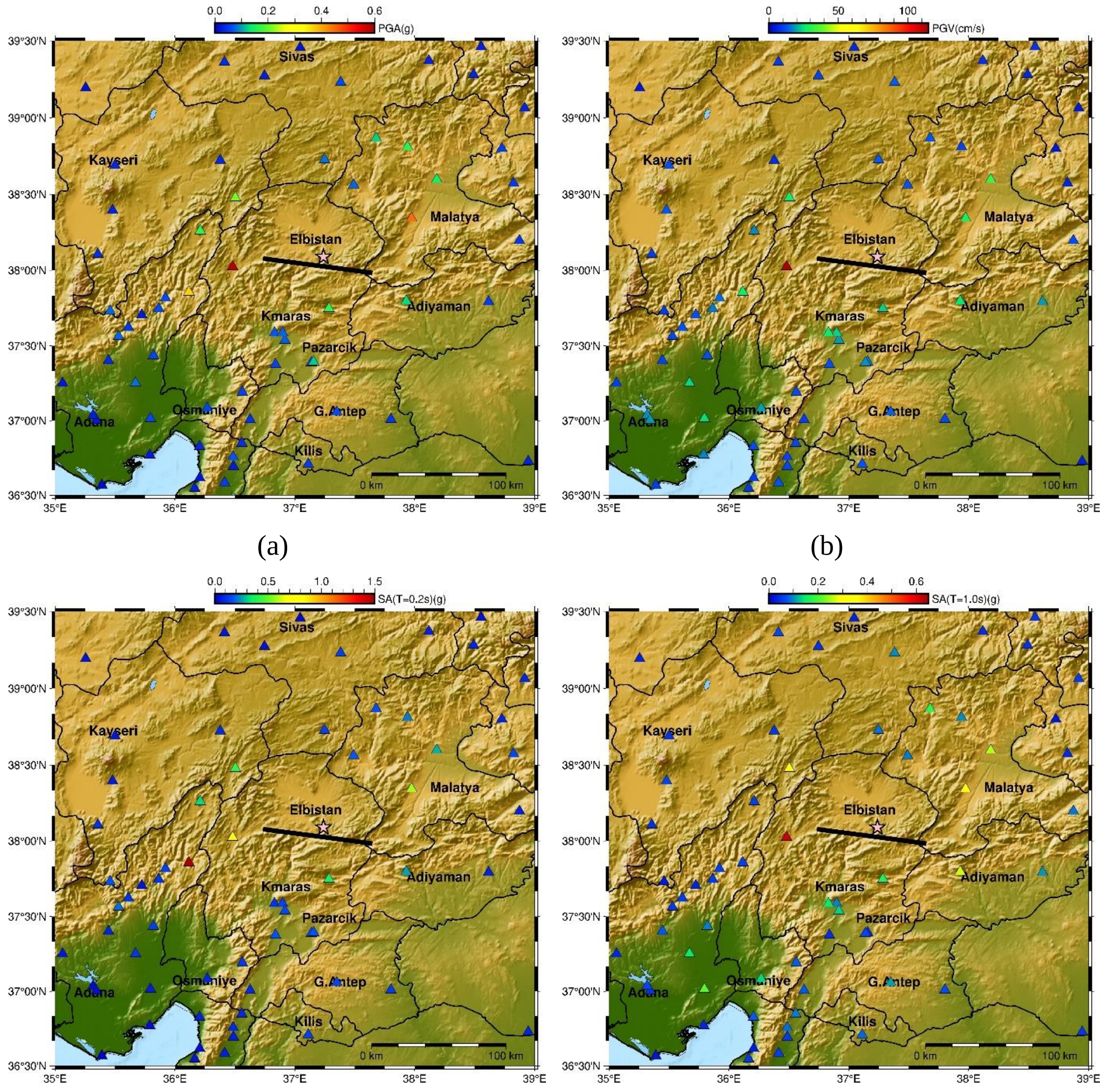

Figure 4.16. Spatial distribution of intensity measure of Elbistan earthquake (a) PGA, (b) PGV, (c) T=0.2 s PSA and (d) T=1.0 s PSA

4.5. Performance of Current Ground Motion Models

Performance evaluation of ground motion models (GMMs) was conducted on a set of selected GMMs that represent the ground motion characteristics of the region. The best representative suit of GMMs for shallow active crustal tectonic regions was determined according to the proposals of Gulerce et al. (2016), Akkar et al. (2018), and Kale (2019), as well as the expert opinions. The final evaluation set includes the following GMMs:

- the local model of Kale et al. (2015) – KAAH15 developed by using the Turkish ground motion dataset,
- the Turkey-adjusted version of the global NGA-W1 Chiou and Youngs (2008) model of Gulerce et al. (2016) - GCY16,
- the regional Pan-European models of Akkar et al. (2014) - ASB14 and Kotha et al. (2022) – KWBC22,
- the global Next Generation Attenuation (NGA) West 2 models of Boore et al. (2014) - BSSA14, and Chiou and Youngs (2014) - CY14.

The evaluations of the selected GMMs are based on the visual inspections between ground-motion model predictions and recorded ground-motion amplitudes. To this end, a subset of the ground motion dataset is compiled by selecting the strong motion stations with measured V_{S30} values, and R_{JB} and R_{RUP} < 300 km for each earthquake (Pazarcik and Elbistan). This distance limit falls within the model applicability ranges of GMMs, except for ASB14 and KAAH15, for which extrapolation of the models is considered. To obtain the model predictions, functional forms of the GMMs require a set of basic estimator parameters such as M_w, R_{JB}, R_{RUP}, V_{S30}, and style-of-faulting, whereas the global model of CY14 considers additional estimator parameters such as horizontal distance to the top edge of rupture measured perpendicular to the strike(R_X), depth-to-top of rupture (Z_{TOR}), dip angle, depth to the shear-wave velocity horizon of 1.0 km⁄s ($Z_{1.0}$), etc. Most of the parameters are computed by considering the ruptured fault plane, whereas the soil sediment parameter ($Z_{1.0}$) is estimated from the empirical relationship proposed by Chiou and Youngs (2014) as a function of V_{S30}.

To assess the distance attenuation of observed ground motions and compare them with the distance scaling of selected GMMs, we present the distribution of the geometric mean of the recordings at PGV, PGA, PSA at T=0.2 s, 1.0 s, and 3.0 s with R_{JB} for the Pazarcik and Elbistan Earthquakes separately. Although the figures show RJB as the distance metric to ensure consistency, the predictions of each GMM are calculated based on the original distance metric definition of the models. The median predictions of the BSSA14 model are calculated by considering the Turkiye-specific regional adjustment term (high-Q option) proposed by Boore et al. (2014). For the figures, recorded ground motions are converted to reference rock site conditions (V_{S30} = 760 m/s) using site amplification factors that are calculated for each recording and each GMM separately.

Figures 4.17 – 4.21 show the comparisons of the Pazarcik Earthquake:

- Recorded PGA values are generally higher than the median estimations of ASB14, KWBC22, and KAAH15 models for R_{RUP}<100km. In this distance range, the recorded motions are almost equally distributed around the median for GCY16, BSSA14, and CY14 models.
- The slope of the distance scaling in the recorded PGAs decays faster than the distance scaling implemented in almost all selected models for R_{RUP}>100km, except for KWBC22. This observation is consistent with the observations from recent large-magnitude events in Turkey (e.g., Samos earthquake, Gülerce et al., 2021), underlining that the large distance scaling of the ground motions recorded in Turkey calls for a critical and in-depth overview.
- Therefore, the event terms should definitely be estimated for an R_{RUP}<100km dataset in the early stages of regression for any future GMMs based on Turkish strong motion data.
- Median predictions of selected GMMs are quite different for PGV, hence the distribution of recorded PGVs with respect to median varies significantly. The median predictions of ASB14 and KAAH15 models are lower than the other models and eventually lower than the recorded motions, especially in the near field. Recorded motions are closer to the median plus one sigma range for the other models. At longer distances, median PGV predictions of all models are quite consistent with the recorded data.
- Predictive performance of all models is significantly good for PSA at T = 0.2 s for R_{RUP}<100km. Faster decay than the models' attenuation is also observed at large distances.
- Median to short distance predictive performance of selected GMMs for PSA at T = 1 s is similar to PGA. However, the distance scaling of GMMs and the distance scaling of 1-s spectral accelerations are very different for R_{RUP}>100km, except for KWBC22 and CY14

models. This observation underlines the need for evaluating the anelastic attenuation terms in the GMMs developed (KAAH15) and calibrated for Turkey (BSSA14 and GCY16).

- At T = 3 s, the predictive performance of BSSA14 and KWBC22 models are superior when compared to the other models. Recorded long-period ground motions are considerable, especially in the near-field region. This preliminary observation calls for a detailed analysis of the potential directivity effects, especially at or near the end of the rupture.

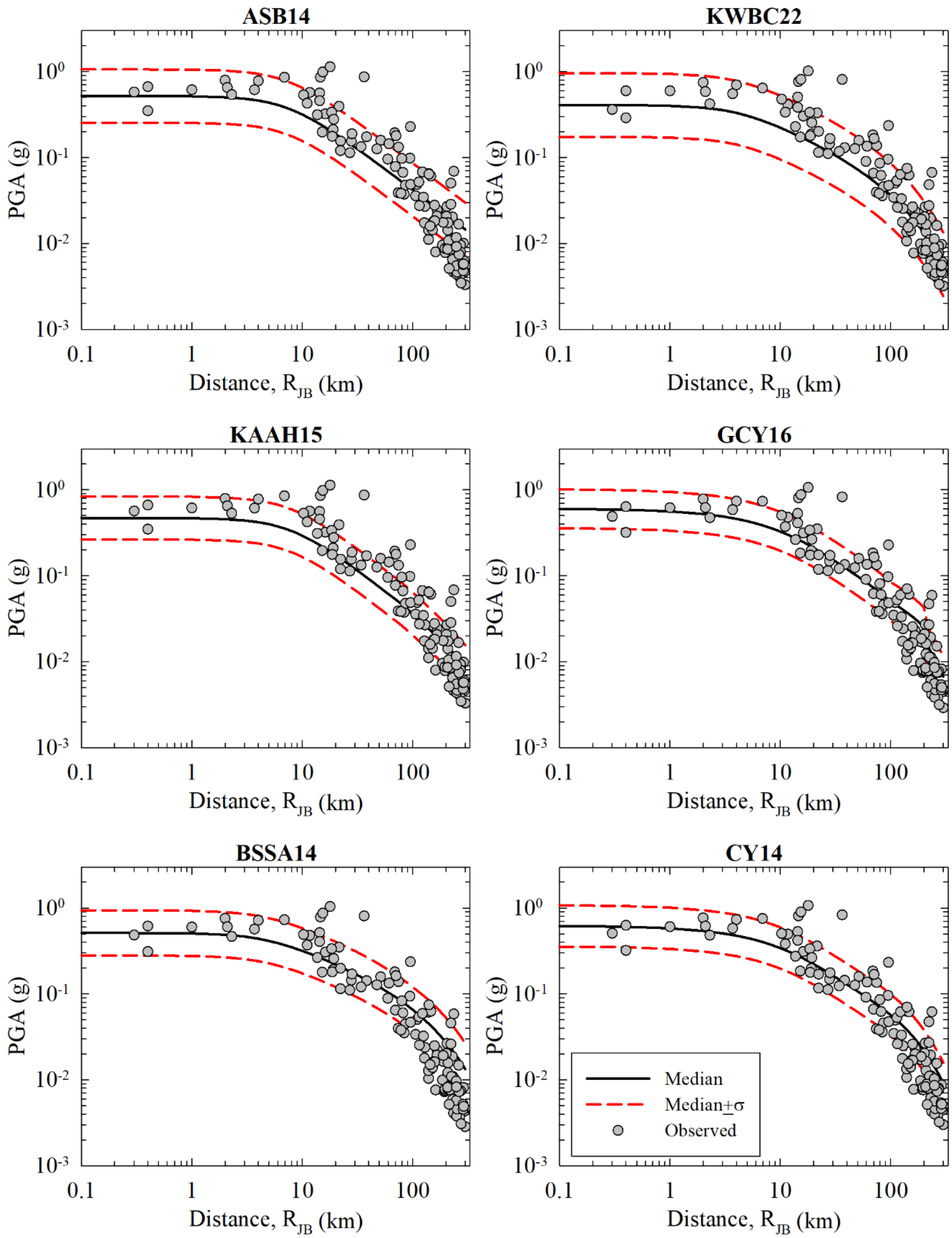

Figure 4.17. Comparison of the distance attenuation of ASB14, KWBC22, KAAH15, GCY16, BSSA14, and CY14 models with recorded strong motion data for PGA. Median and median ±1σ curves are given with black solid and red dashed lines, respectively. Gray points represent the V_{S30} normalized recorded strong motion data for Pazarcik Earthquake.

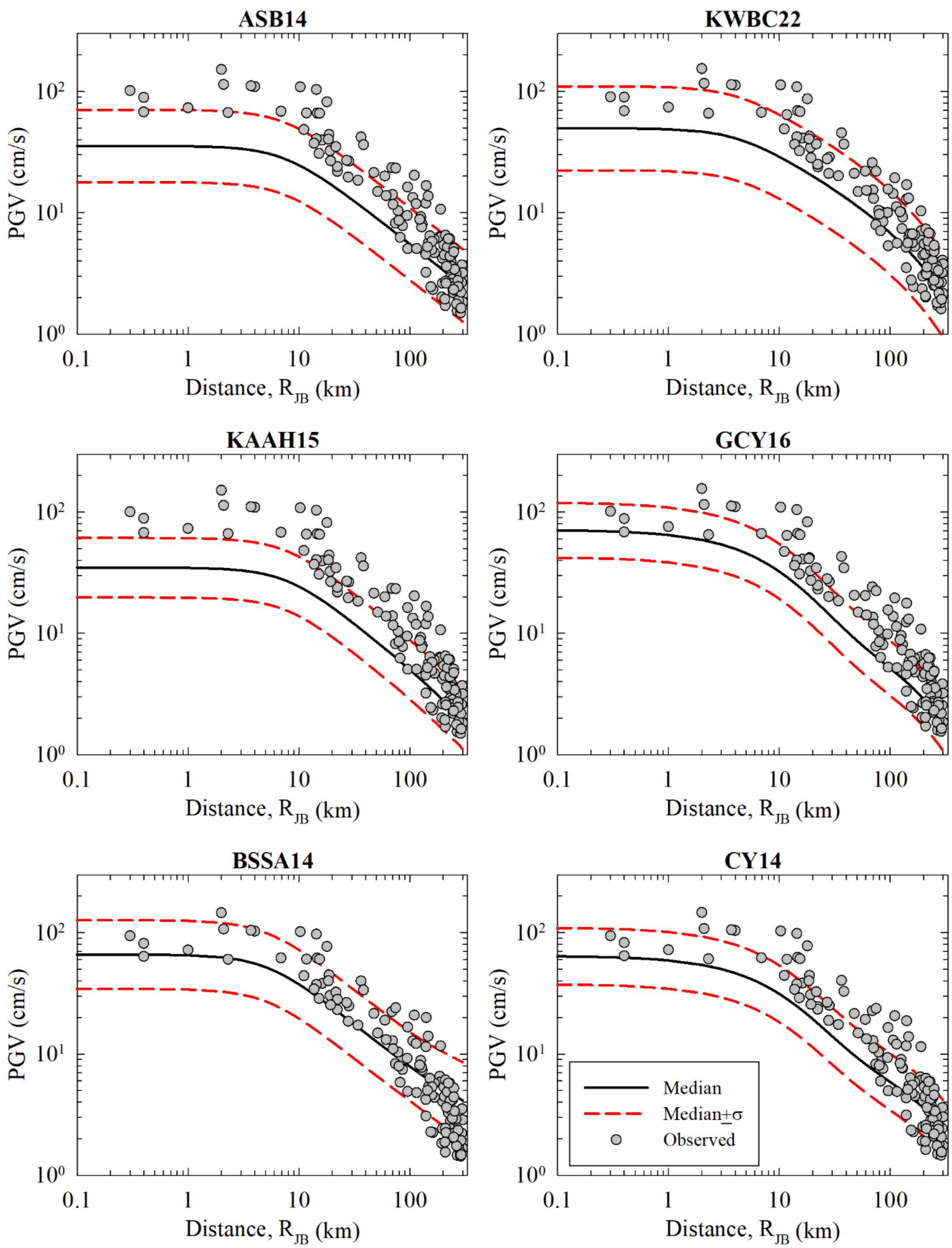

Figure 4.18. Comparison of the distance attenuation of ASB14, KWBC22, KAAH15, GCY16, BSSA14, and CY14 models with recorded strong motion data for PGV. Median and median ±1σ curves are given with black solid and red dashed lines, respectively. Gray points represent the V_{S30} normalized recorded strong motion data for Pazarcik Earthquake.

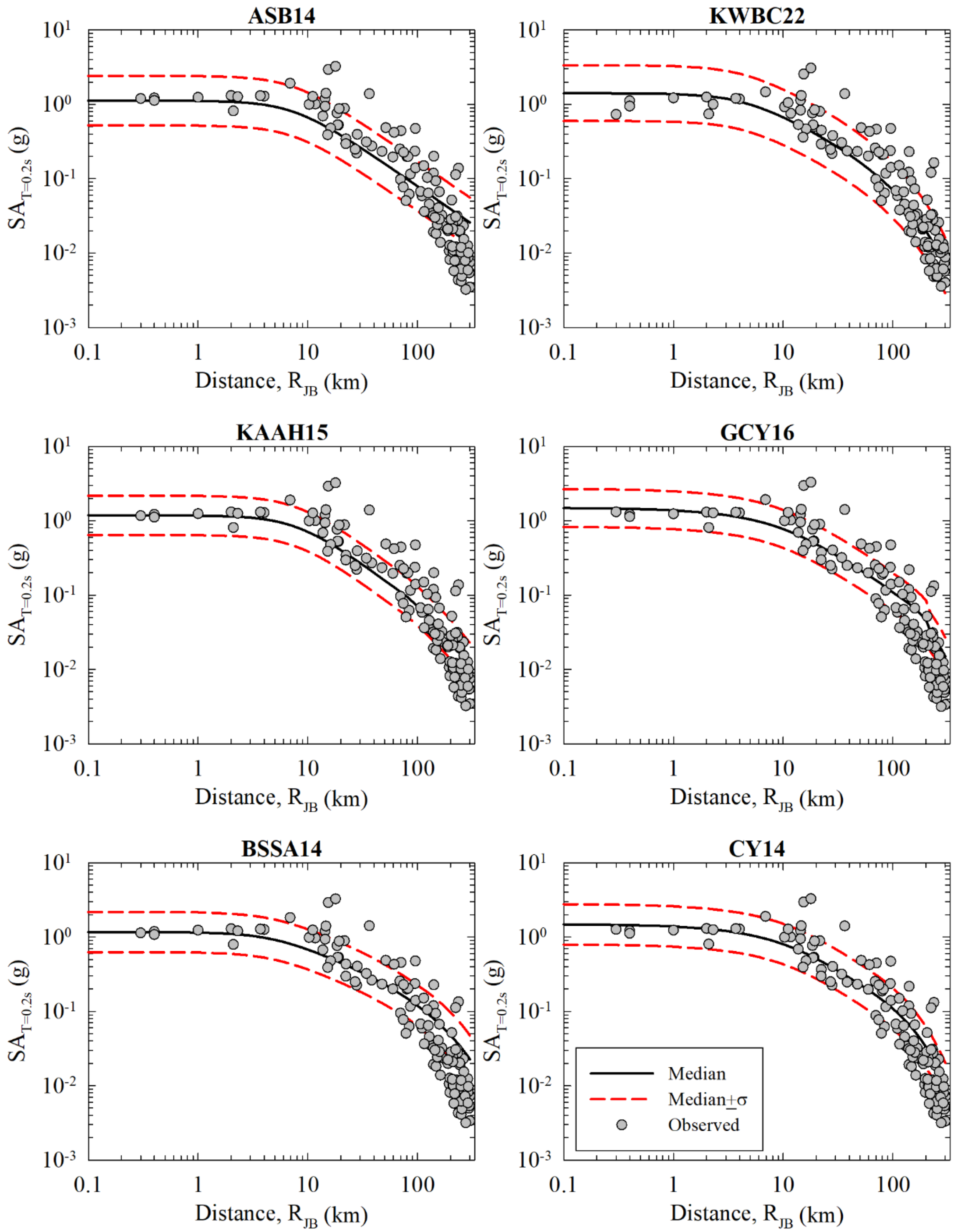

Figure 4.19. Comparison of the distance attenuation of ASB14, KWBC22, KAAH15, GCY16, BSSA14, and CY14 models with recorded strong motion data for T=0.2s PSA. Median and median ±1σ curves are given with black solid and red dashed lines, respectively. Gray points represent the V_{S30} normalized recorded strong motion data for Pazarcik Earthquake.

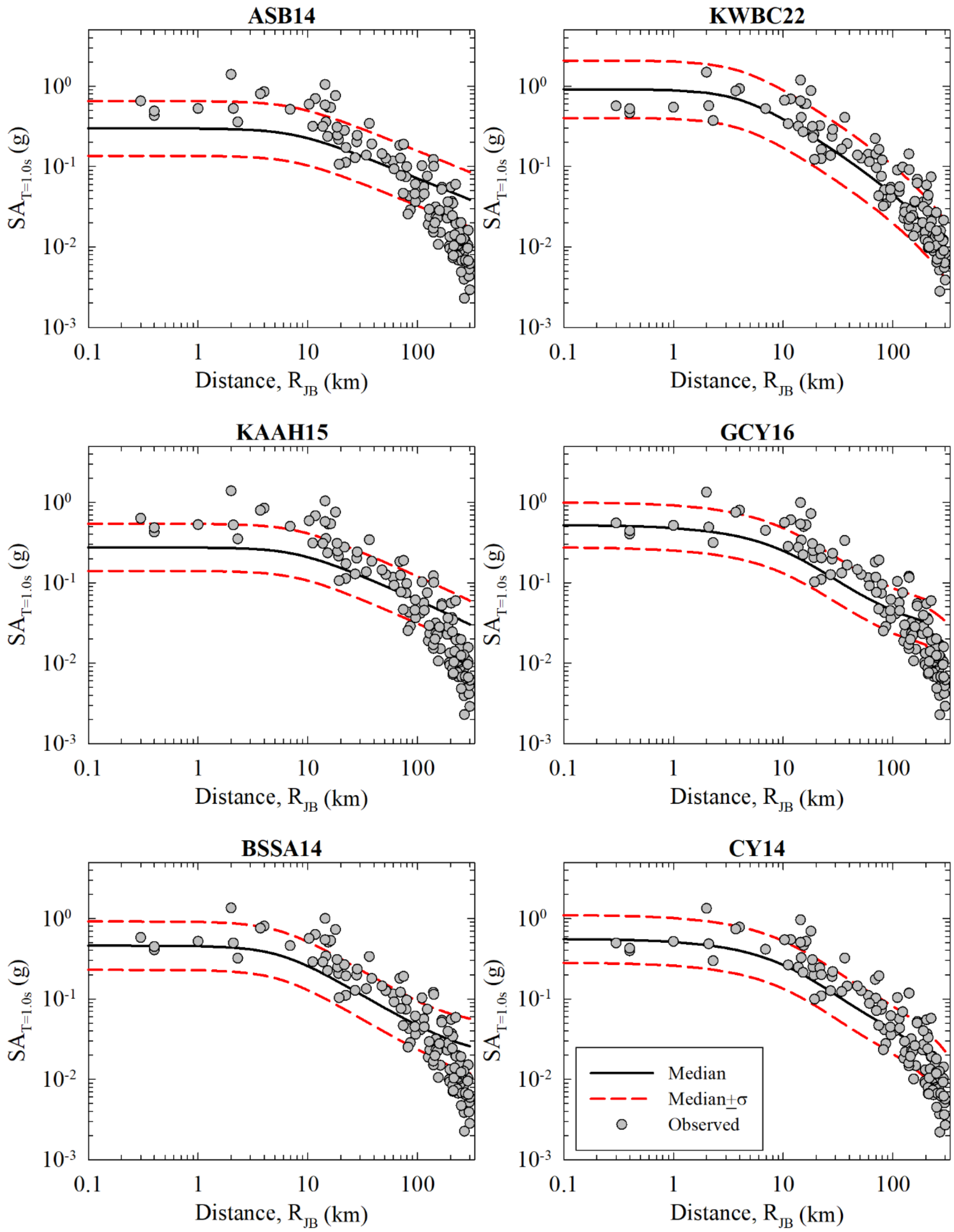

Figure 4.20. Comparison of the distance attenuation of ASB14, KWBC22, KAAH15, GCY16, BSSA14, and CY14 models with recorded strong motion data for T=1.0s PSA. Median and median ±1σ curves are given with black solid and red dashed lines, respectively. Gray points represent the V_{S30} normalized recorded strong motion data for Pazarcik Earthquake.

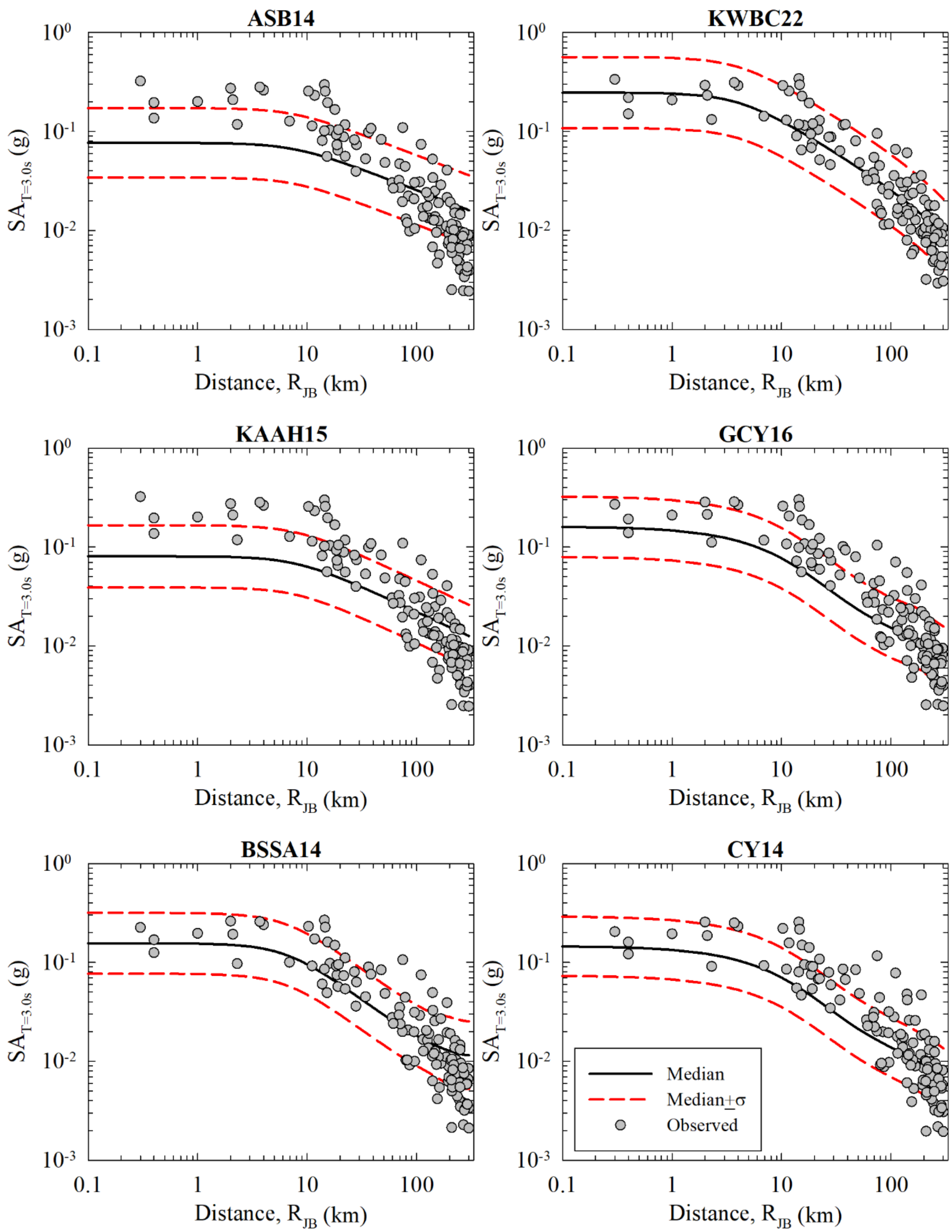

Figure 4.21. Comparison of the distance attenuation of ASB14, KWBC22, KAAH15, GCY16, BSSA14, and CY14 models with recorded strong motion data for T=3.0s PSA. Median and median ±1σ curves are given with black solid and red dashed lines, respectively. Gray points represent the V_{S30} normalized recorded strong motion data for Pazarcik Earthquake.

Figures 4.22 to 4.26 show the comparisons of the Elbistan Earthquake:

- The number of stations within the first 50 km of the rupture (that have passed the quality check) is very limited. Therefore, it is not meaningful to reach any conclusions on the geometrical spreading (short distance scaling) for this event.
- Except for a few outlying stations, the recordings at the R_{RUP}=50-100 km are generally in good agreement with the median predictions of the selected GMMs at all spectral periods, except for PGV.
- Interpretations for the first event, related to the large distance scaling, are also valid for this event. The large distance slope of the recordings is inconsistent with the large distance slope of almost all GMMs. The large distance predictive performance of CY14 and KWBC22 is superior to the other models at certain periods.
- Recorded PGV values are higher than the median predictions of all selected GMMs. The difference between the actual data and median estimations is most prominent for KAAH15 and GCY16 models, which were developed or calibrated by using Turkish strong motion recordings. This observation is striking and not easy to explain with the possible directivity effects.
- Recorded PGV values are larger than the median (or even larger than the median plus one sigma) but the long-period ground motions (PSA T = 1.0 s and PSA T = 3.0 s) are well distributed around the median for most models. This also supports the lack of long-period directivity pulse in the recorded motions.

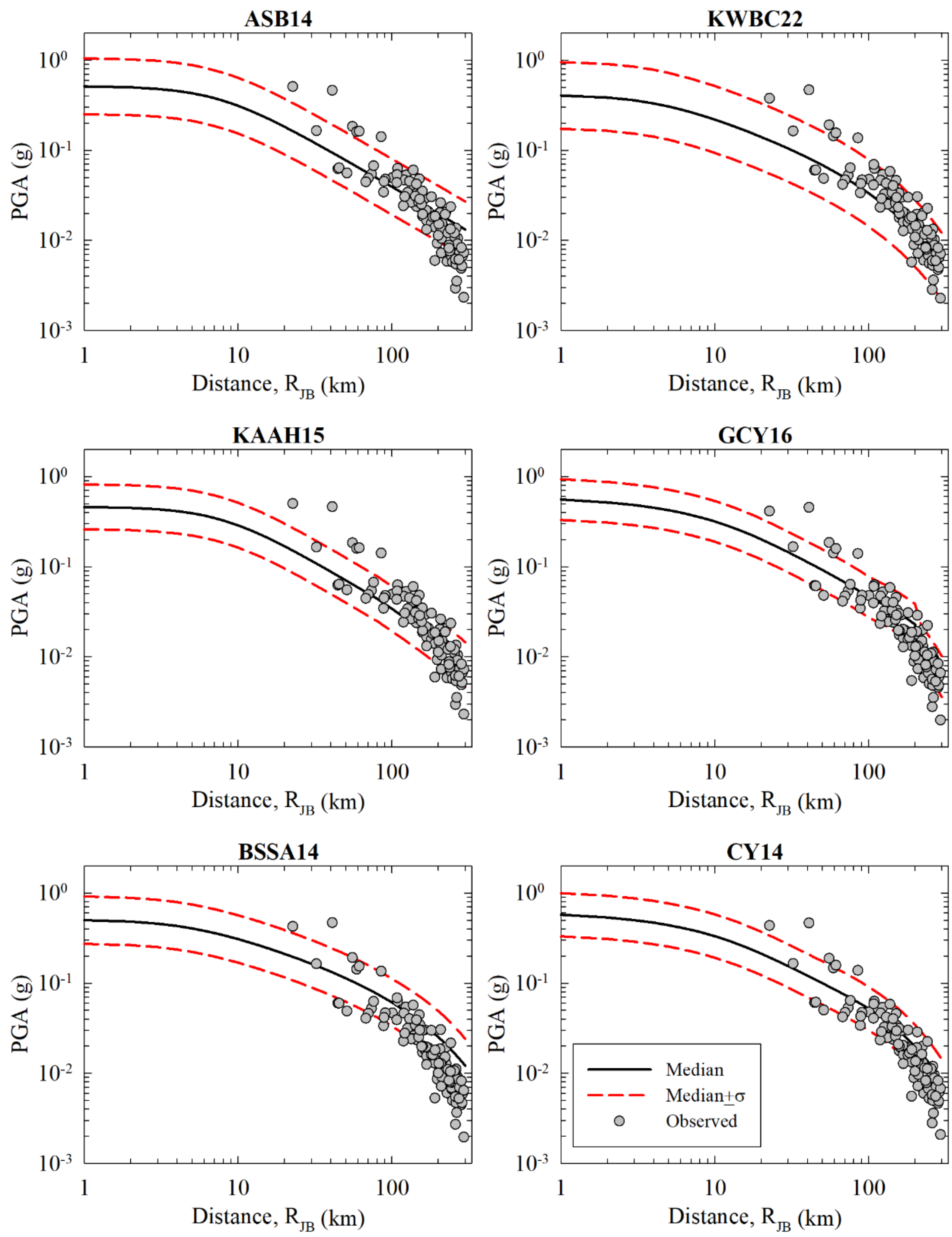

Figure 4.22. Comparison of the distance attenuation of ASB14, KWBC22, KAAH15, GCY16, BSSA14 and CY14 models with recorded strong motion data for PGA. Median and median ±1σ curves are given with black solid and red dashed lines, respectively. Gray points represent the V_{S30} normalized recorded strong motion data for Elbistan Earthquake.

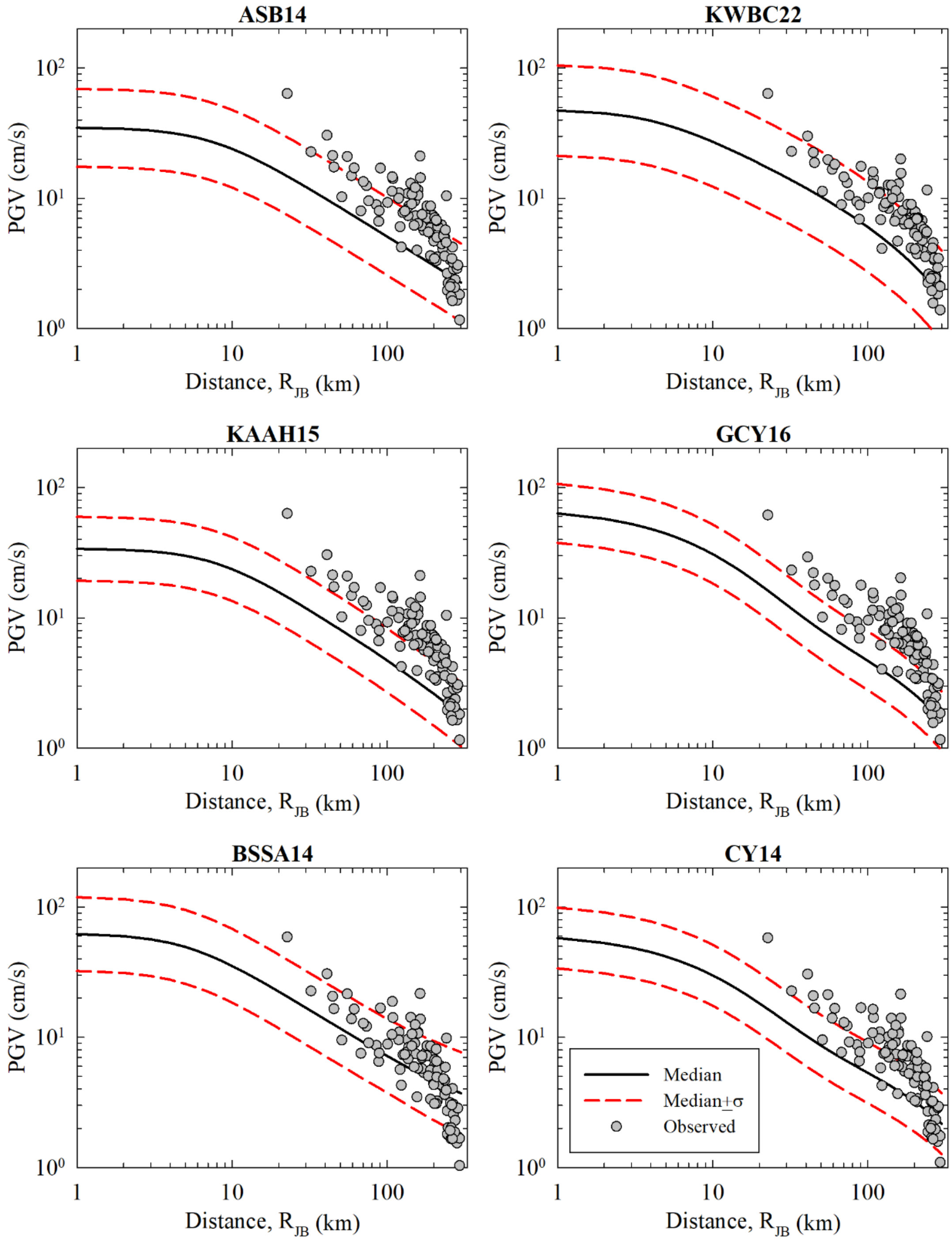

Figure 4.23. Comparison of the distance attenuation of ASB14, KWBC22, KAAH15, GCY16, BSSA14 and CY14 models with recorded strong motion data for PGV. Median and median ±1σ curves are given with black solid and red dashed lines, respectively. Gray points represent the V_{S30} normalized recorded strong motion data for Elbistan Earthquake.

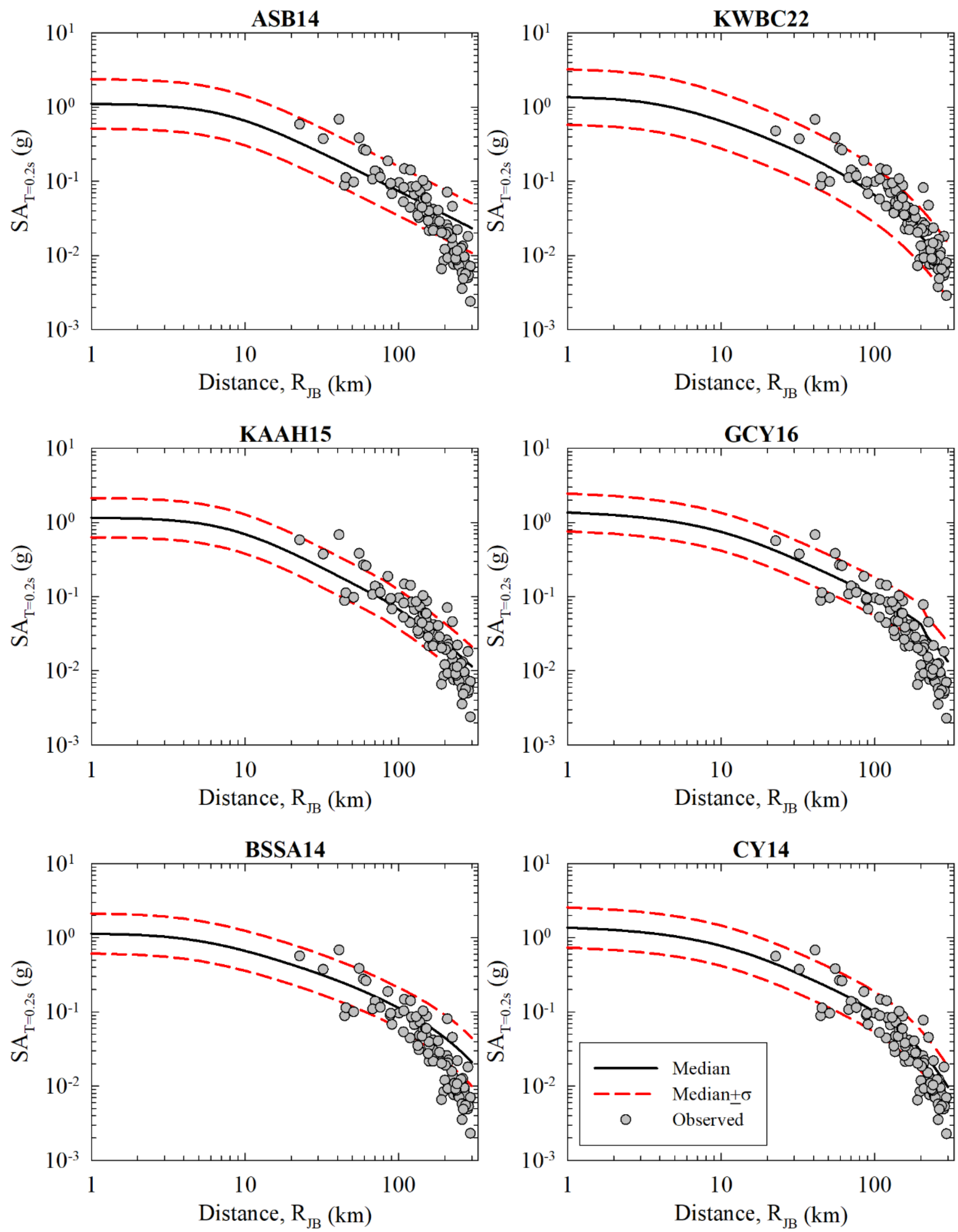

Figure 4.24. Comparison of the distance attenuation of ASB14, KWBC22, KAAH15, GCY16, BSSA14 and CY14 models with recorded strong motion data for T=0.2s PSA. Median and median ±1σ curves are given with black solid and red dashed lines, respectively. Gray points represent the V_{S30} normalized recorded strong motion data for Elbistan Earthquake.

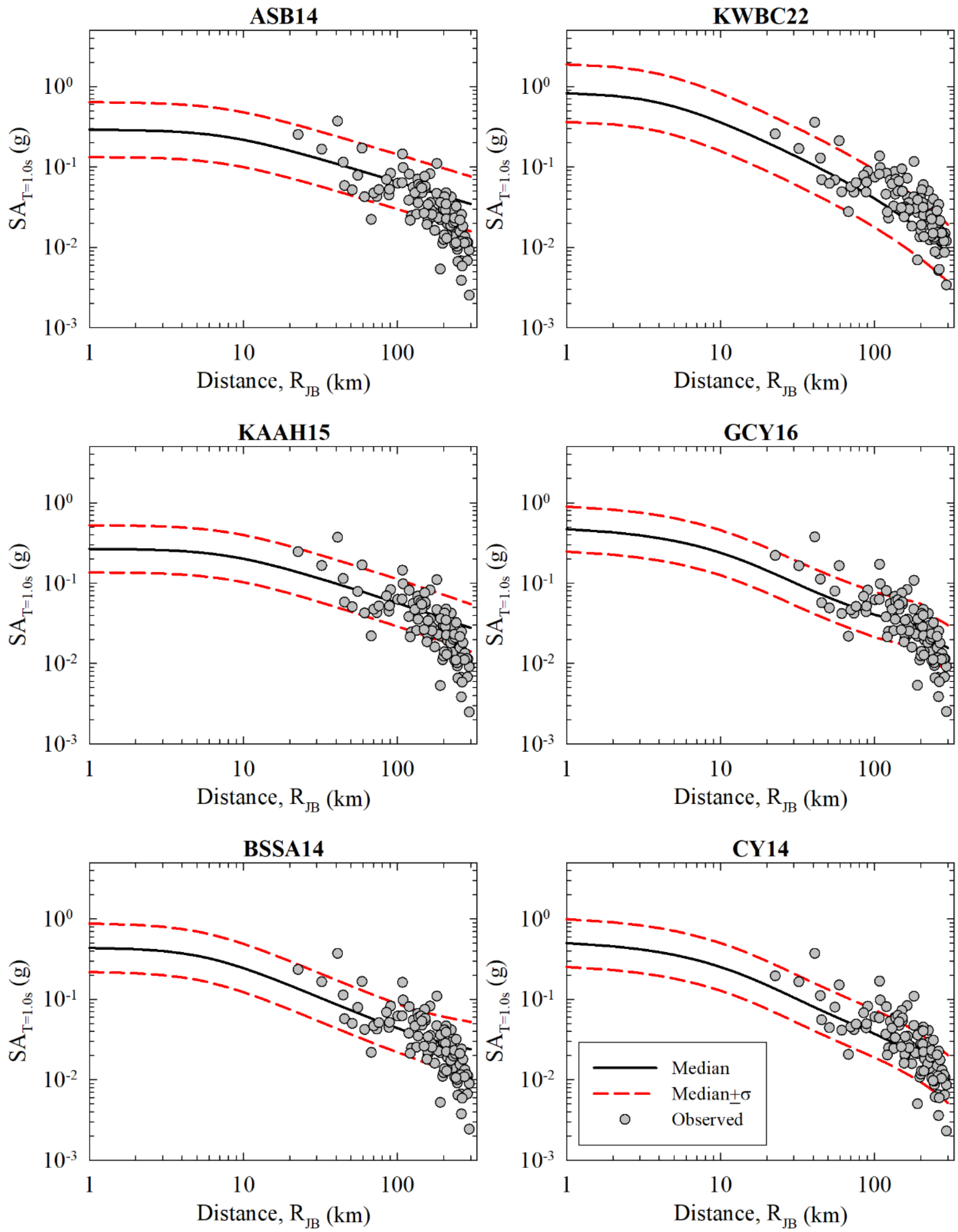

Figure 4.25. Comparison of the distance attenuation of ASB14, KWBC22, KAAH15, GCY16, BSSA14 and CY14 models with recorded strong motion data for T=1.0s PSA. Median and median ±1σ curves are given with black solid and red dashed lines, respectively. Gray points represent the V_{S30} normalized recorded strong motion data for Elbistan Earthquake.

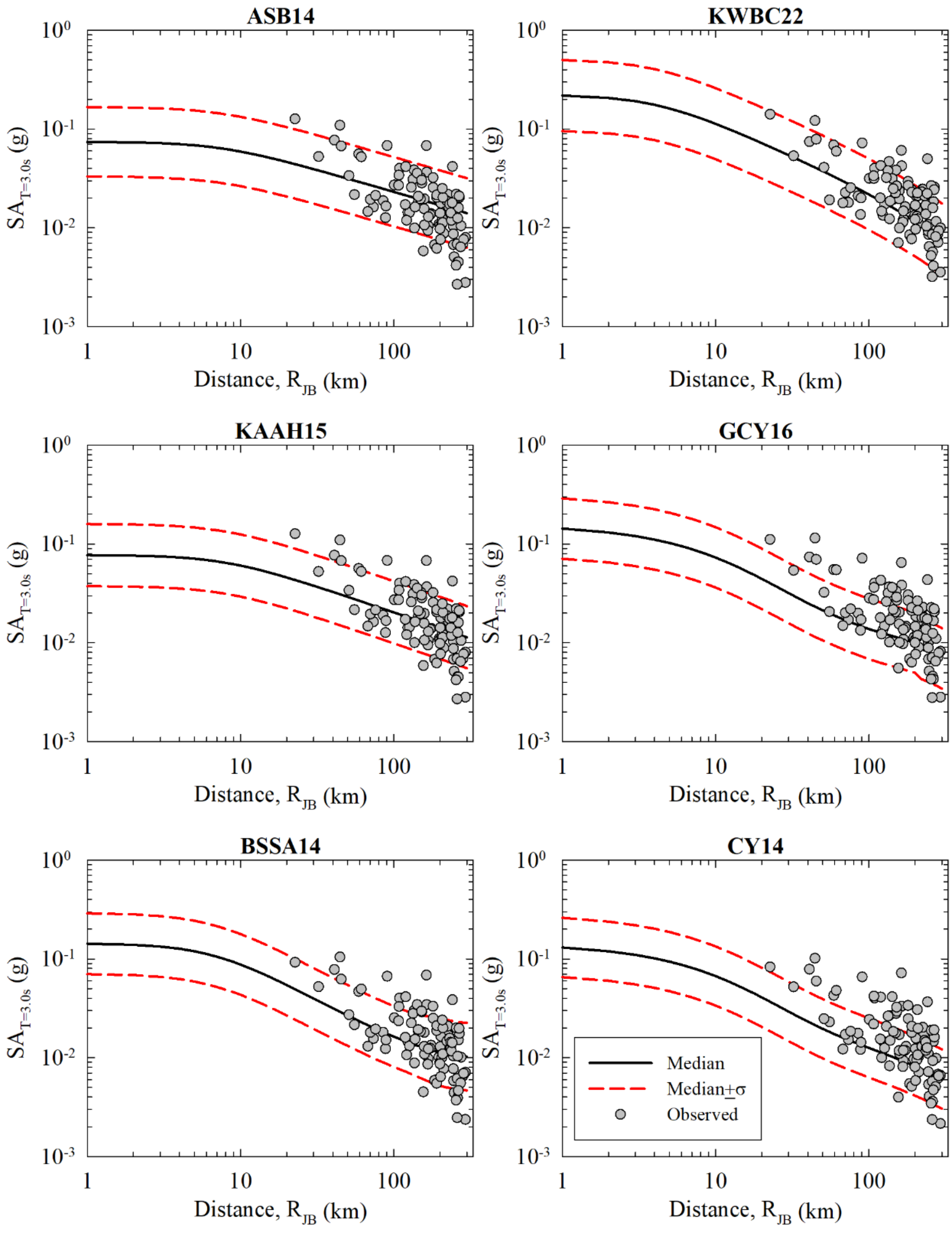

Figure 4.26. Comparison of the distance attenuation of ASB14, KWBC22, KAAH15, GCY16, BSSA14 and CY14 models with recorded strong motion data for T=3.0s PSA. Median and median ±1σ curves are given with black solid and red dashed lines, respectively. Gray points represent the V_{S30} normalized recorded strong motion data for Elbistan Earthquake.

4.6. Spectral Amplifications and HVSR

Site amplification effects can significantly change the amplitude and frequency content of recorded ground motions. Various methods exist for calculating site amplifications and fundamental periods and frequency values of sites, which include both theoretical and empirical approaches. In this preliminary report, due to the limited availability of field investigation data (shear wave velocity measurement, soil profiles, etc.), the empirical HVSR method, also known as Nakamura's method, is used. This approach was developed by Nakamura (1989) following the original study of Nogoshi and Igarashi (1971). As part of this report, preliminary Horizontal-to-Vertical Spectral Ratio (HVSR) analyses are conducted using recorded strong motion data from selected stations located in Hatay, Gaziantep, and Kahramanmaraş after the M_w=7.7 Pazarcik earthquake on 6th February 2023.

HVSR method was originally developed for microtremor recordings, however, it can also be employed using single strong ground motion station measurements to estimate the natural resonant frequencies of near-surface layers. The fundamental assumption in this method is that the vertical motion remains constant during its propagation to the surface, while the horizontal component amplifies or deamplifies due to site response. HVSR spectra are calculated by selecting the S-wave portion of the acceleration record, and FAS is computed for the two horizontal and vertical components at the surface. FAS for the S-wave portion is initially smoothed by Konno and Ohmachi (1998). Next, the geometric mean of the two smoothed horizontal component FAS is divided by the vertical component smoothed FAS to obtain HVSR. at the location. The resulting HVSR curve typically exhibits one or more peaks that correspond to the resonant frequencies of the subsurface layers.

HVSR curves are presented at five selected stations (Stations 2708, 3126, 3138, 4615, and 4624) located near the fault ruptures in Gaziantep, Kahramanmaraş, and Hatay. The selected stations are also shown in Figure 4.5a with a red rectangle.

HVSR values are calculated using Pizzaro (2017) HOVSR (Version 2.0) MATLAB code. Figure 4.27 – 4.31 present the acceleration time histories recorded at the stations and the corresponding HVSR curves, along with V_{s30} and rupture distances. It is observed that for the M_w=7.7 Pazarcik event, there are multiple wave packets. This is extensively discussed in Sections 4.2 and 4.3. This observation is also clearly recognized at stations 2708, 4615, and 4624, where the HVSR values from different S-wave packets are evaluated separately (named as 1st and 2nd packets on the corresponding HVSR curves).

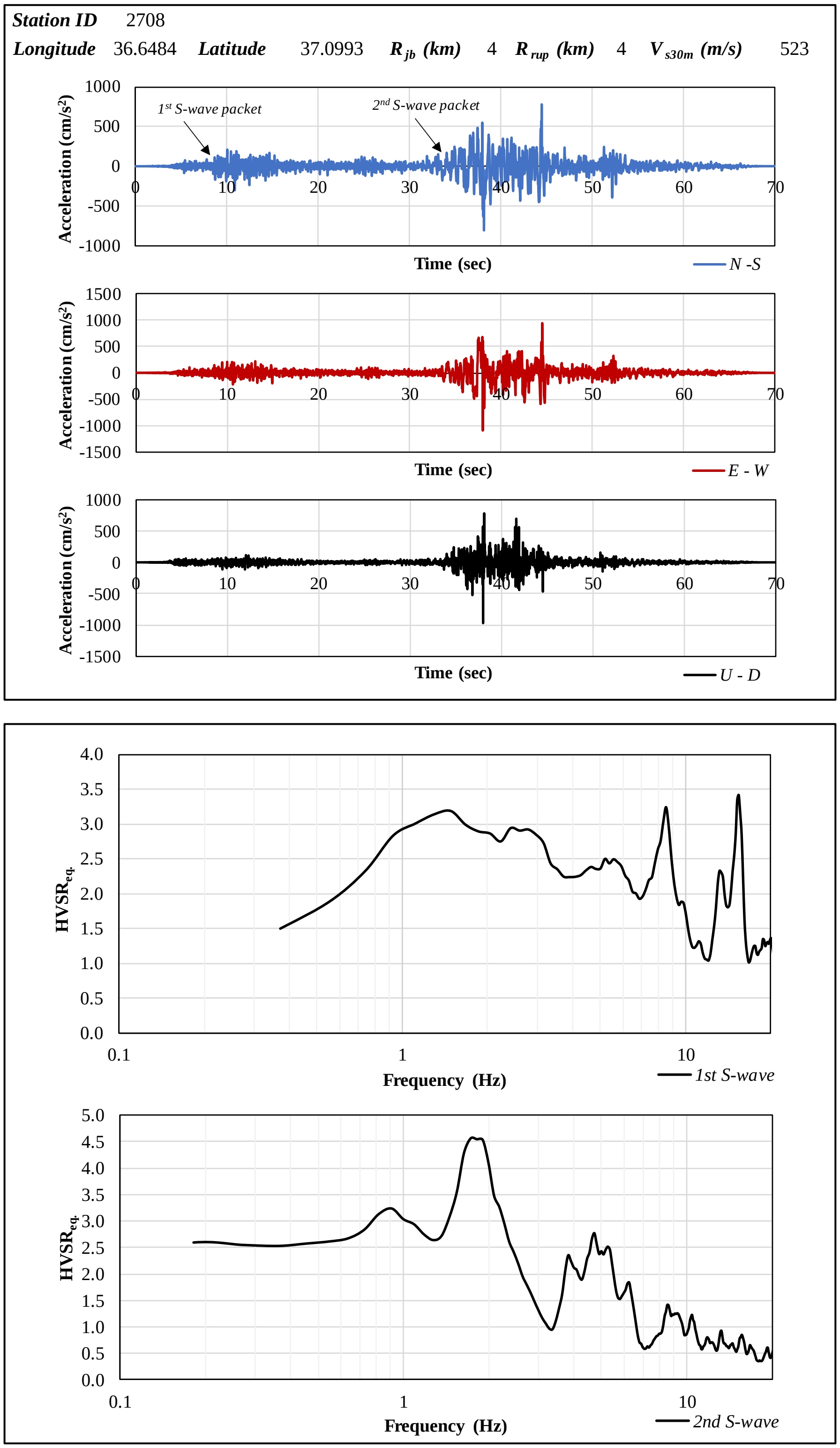

Figure 4.27. Resulting HVSR curve for station 2708

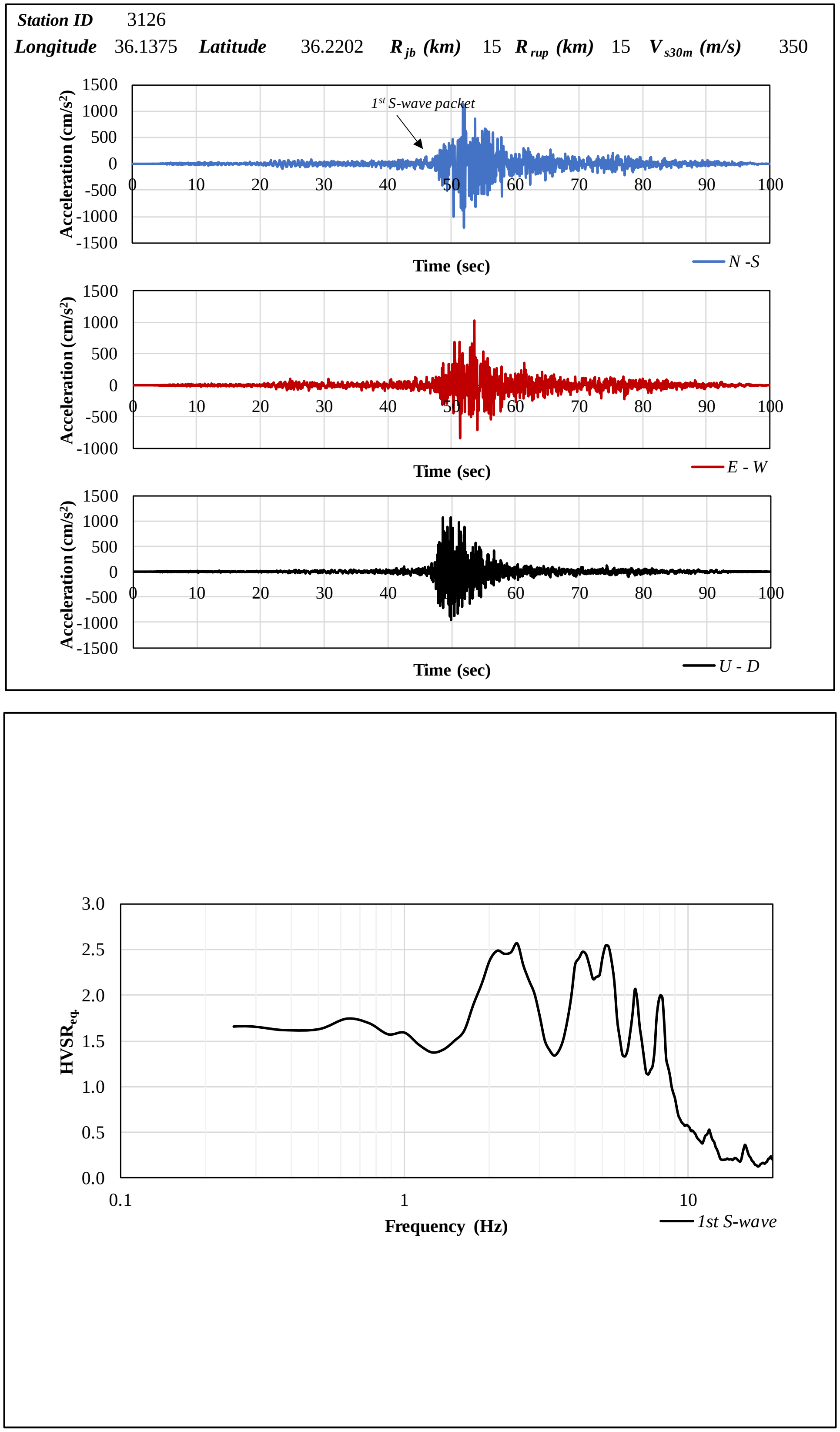

Figure 4.28. Resulting HVSR curve for station 3126

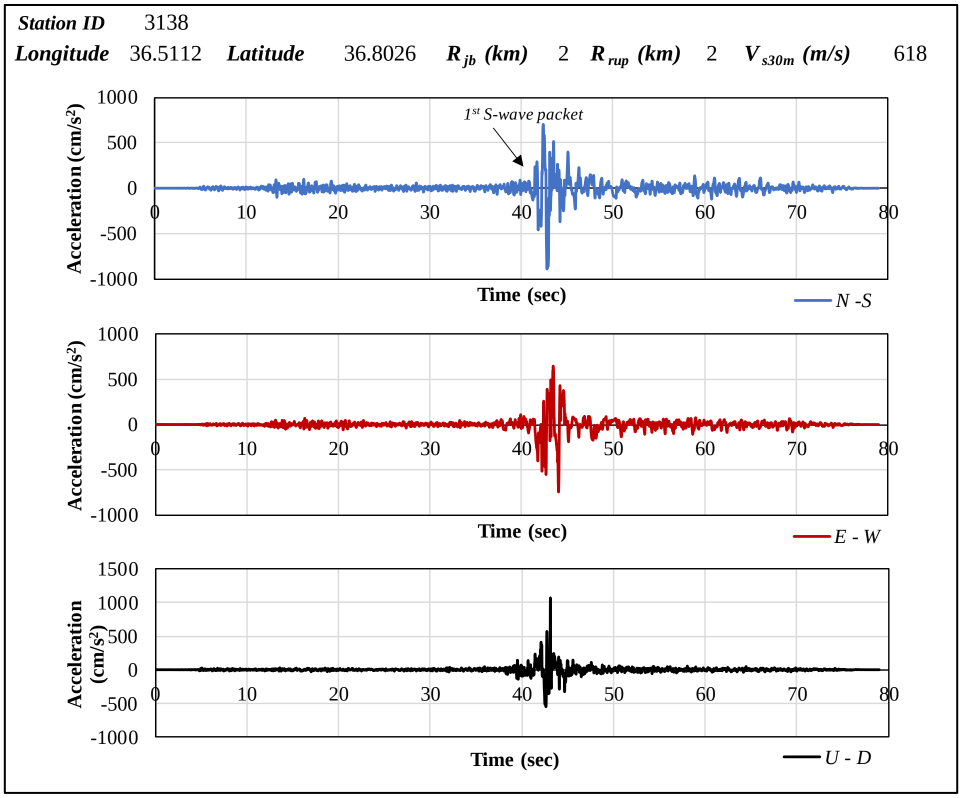

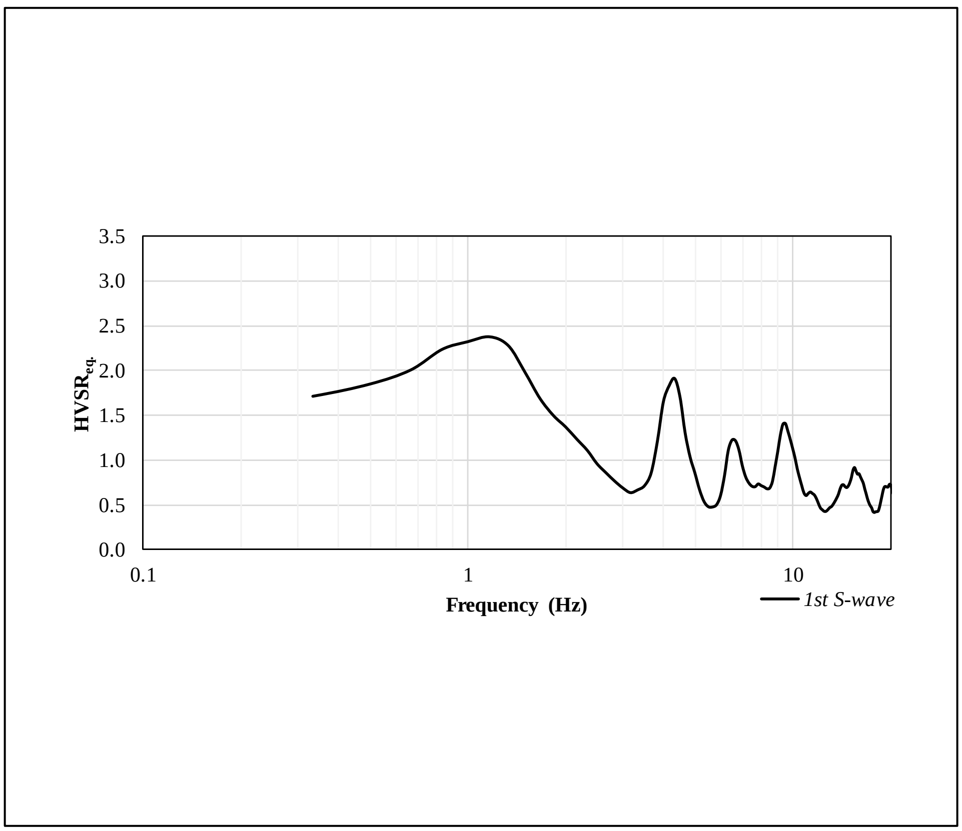

Figure 4.29. Resulting HVSR curve for station 3138

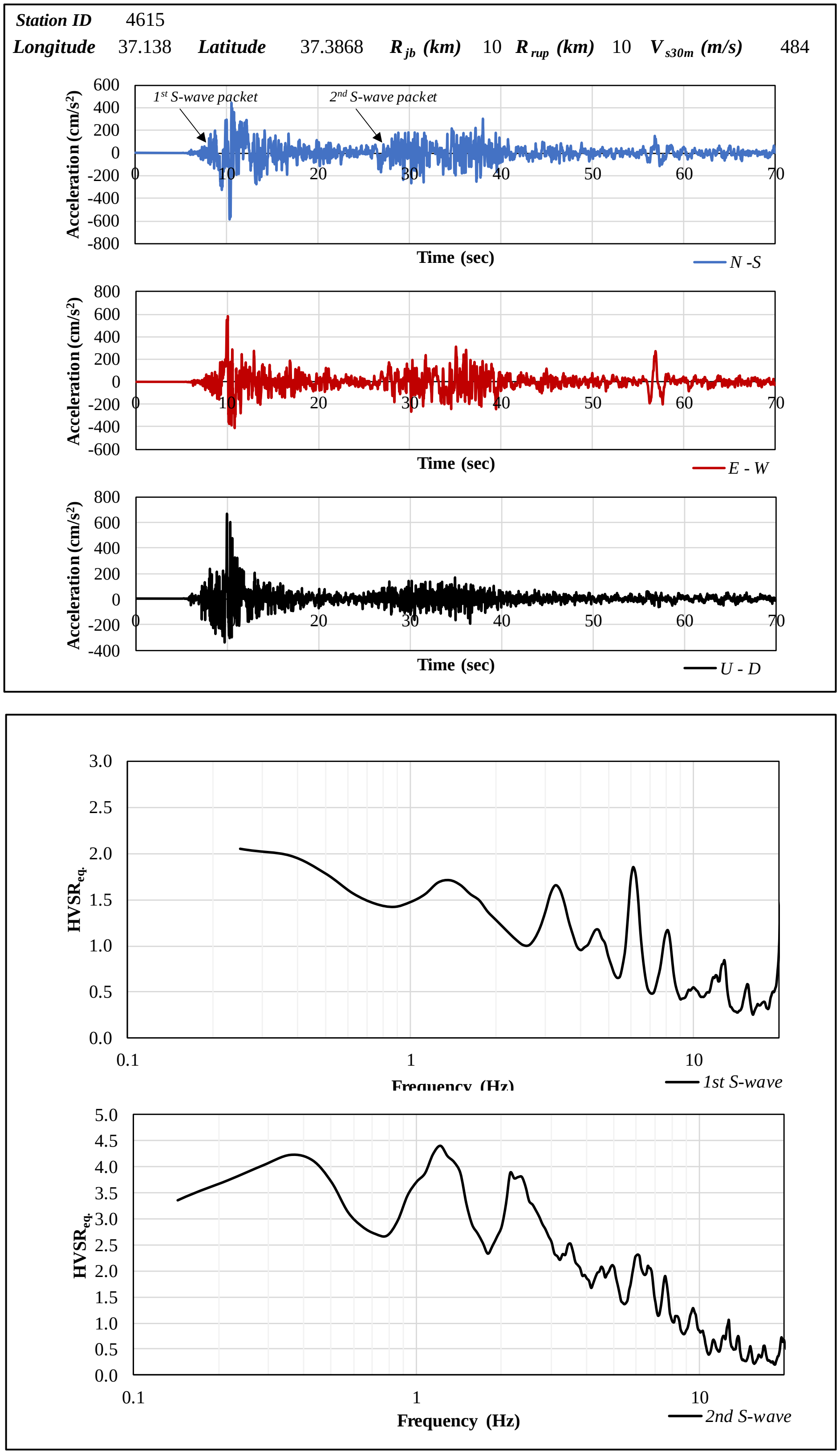

Figure 4.30. Resulting HVSR curve for station 4615

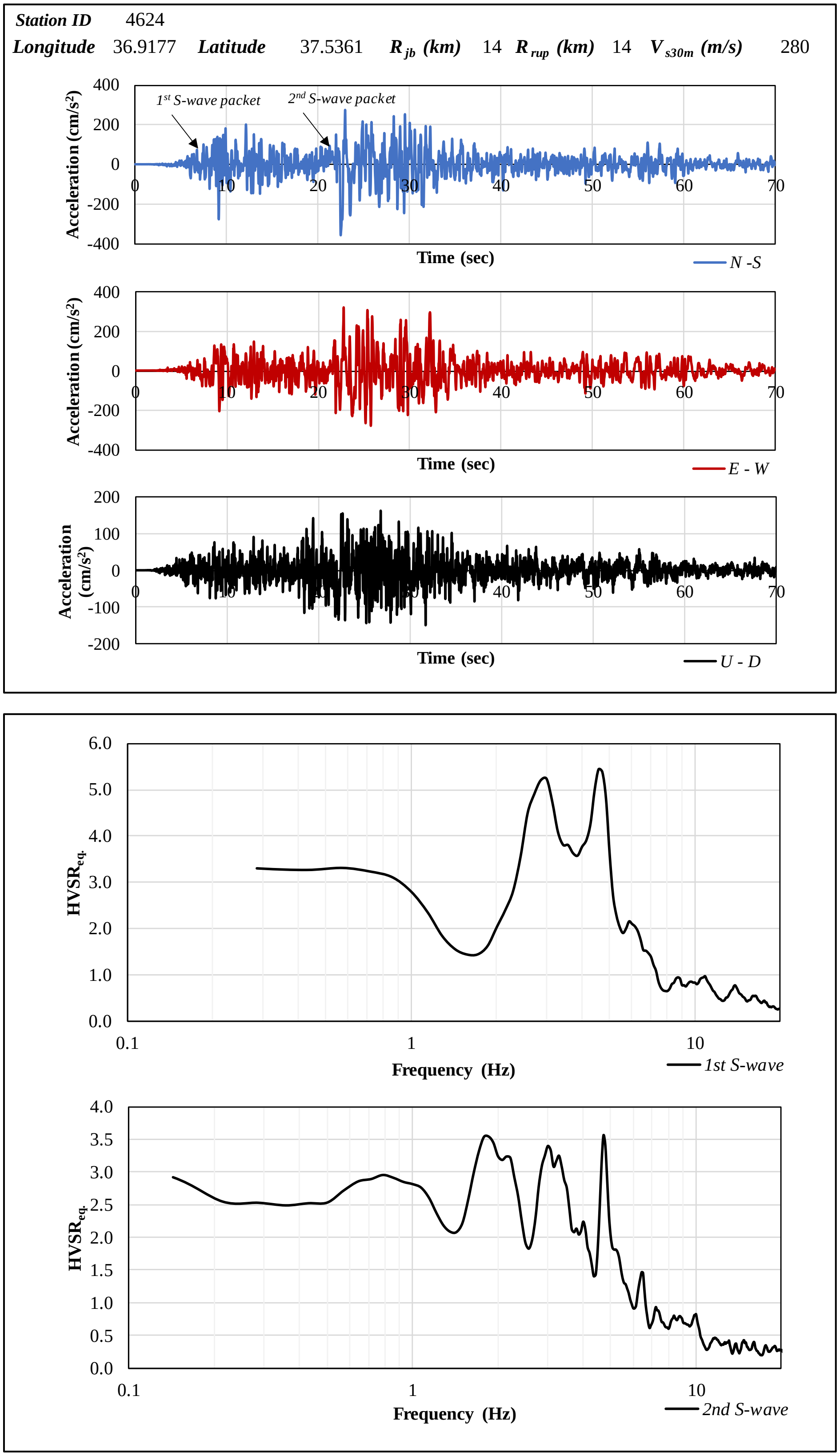

Figure 4.31. Resulting HVSR curve for station 4624

HVSR curves are commonly used to estimate the fundamental frequency values of sites, but their effectiveness in evaluating site amplifications is still being debated in the literature. To better assess site amplifications in future evaluations, amplification ratios using either the standard spectral ratio method (SSR), which normalizes outcrop soil response spectra to the nearest rock outcrop motion, or site-specific 1-D site response analyses at the selected stations. More specifically,

- Station 2708 (Figure 4.27) is located on either a very dense soil or a very soft rock site, where the $V_{s,30m}$ is 523 m/s and HVSR indicates peaks around 1.5 Hz (T=0.67 sec) and 7.5 Hz (T=0.13 sec) for the 1st S-wave portion and relatively low frequency 1.9 Hz (T=0.53 sec) and 5.0 Hz (T=0.2 sec) peak for the 2nd S-wave portion.
- Station 3126 (Figure 4.28) is located on a stiff soil site, where the $V_{s,30m}$ is 350 m/s and HVSR indicates peaks around 2.4 Hz (T=0.42 sec) and 5.3 Hz (T=0.19 sec).
- Station 3138 (Figure 4.29) is located on either a very dense soil or a very soft rock site, where the $V_{s,30m}$ is 618 m/s and HVSR indicates peaks around 1.2 Hz (T=0.83 sec) and 4.3 Hz (T=0.23 sec).
- Station 4615 (Figure 4.30) is located on either a very dense soil or a very soft rock site, where the $V_{s,30m}$ is 484 m/s and HVSR indicates peaks around 1.5 Hz (T=0.67 sec) and 2.5 (T=0.4 sec) Hz for the 1st S-wave portion and relatively low frequency 0.4 Hz (T=2.5 sec) and 1.2 Hz (T=0.83 sec) peak for the 2nd S-wave portion.
- Station 4624 (Figure 4.31) is located on a stiff soil site, classified as a NERHP Site Class D ($V_{s,30m}$ = 280 m/s) and HVSR indicates peaks around 3 Hz (T=0.33 sec) and 5 Hz (T=0.2 sec) for the 1st S-wave packet and relatively low frequency 0.8 Hz (T=1.25 sec) and 2 Hz (T=0.5 sec) peak for the 2nd S-wave packet.

To summarize, when the HVSR is assessed from the first and second wave packets, different fundamental frequencies are estimated. This suggests a shift in site periods, which could be attributed to strain-dependent softening of individual soil layers, as well as the softening of the overall site. These factors, along with others are to be studied as part of more in-depth site response assessments. The use of the entire time series in the development of HVSR curves may have produce a wider range of amplified frequencies, which also requires further evaluations

4.7. References

Akkar, S., Sandıkkaya, M.A., Şenyurt, M., Azari Sisi, A., Ay, B.Ö., Treversa, P., Douglas, J., Cotton, F., Luzi, L., Hernandez, B., Godey, S. 2014. "Reference Database for Seismic Ground Motion in Europe (RESORCE)". Bulletin of Earthquake Engineering, 12:311–339. https://doi.org/10.1007/s10518-013-9506-8

Akkar, S., Sandikkaya, M. A., Bommer, J. J. 2014c. "Empirical ground-motion models for point- and extended-source crustal earthquake scenarios in Europe and the Middle East". Bulletin of Earthquake Engineering, 12: 359–387. https://doi.org/10.1007/s10518-013-9461-4

Akkar, S., Kale, Ö., Yakut, A., Çeken, U. 2018. "Ground-motion characterization for the probabilistic seismic hazard assessment in Turkey", Bulletin of Earthquake Engineering, 16: 3439–3463. https://doi.org/10.1007/s10518-017-0101-2

Albayrak, K., Askan, A., Yerlikaya, F. 2023. "Ground Motion to Intensity Conversion Equations (GMICEs) for Turkey: Evaluation of Regional Differences with Parametric and Non-Parametric Regression Methods", [Working paper].

ASCE 7-16 (2017). "Minimum Design Loads and Associated Criteria for Buildings and Other Structures in Seismic Design Requirements for Building Structures: Structural Engineering Institute" (pp. 89-121). https://doi.org/10.1061/9780784414248

Atkinson, G., Silva, W., 2000. "Stochastic Modeling of California Ground Motions". Bulletin of the Seismological Society of America, 90(2), pp.255-274. https://doi.org/10.1785/0119990064

Bilal, M., Askan, A. 2014. "Relationships between felt intensity and recorded ground-motion parameters for Turkey". Bulletin of the Seismological Society of America, 104:1. https://doi.org/10.1785/0120130093

Boore, D. M., Bommer, J. J., 2005. "Processing of strong-motion accelerograms: needs, options and consequences". Soil Dynamics and Earthquake Engineering, 25 93-115. https://doi.org/10.1016/j.soildyn.2004.10.007

Boore, D. M., Sisi, A. A., Akkar, S. 2012. "Using pad-stripped acausally filtered strong-motion data". Bulletin of the Seismological Society of America, 102751-760. https://doi.org/10.1785/0120110222

Boore, D. M., Stewart, J. P., Seyhan, E., Atkinson, G. M. 2014. "NGA-West 2 equations for predicting PGA, PGV, and 5%-damped PSA for shallow crustal earthquakes". Earthquake Spectra, 30: 1057–1085. https://doi.org/10.1193/070113EQS184M

Building Seismic Safety Council (BSSC) 2020. " NEHRP Recommended Seismic Provisions for New Buildings and Other Structures 2020 Edition". FEMA P-2082, Washington, D.C.

Chiou, B. S.-J., Youngs, R. R. 2008. "An NGA Model for the Average Horizontal Component of Peak Ground Motion and Response Spectra", Earthquake Spectra; 24: 1: 173–215. https://doi.org/10.1193/1.2894832

Chiou, B. S.-J., Youngs, R. R. 2014. "Update of the Chiou and Youngs NGA model for the average horizontal component of peak ground motion and response spectra". Earthquake Spectra, 30: 1117–1153. https://doi.org/10.1193/072813EQS219M

Douglas, J. 2003. "What is a poor quality strong-motion record?". Bulletin of Earthquake Engineering, 1: 141-56. https://doi.org/10.1023/A:1024861528201

Douglas, J, Boore, D.M. 2011. "High-frequency filtering of strong-motion records". Bulletin of Earthquake Engineering, 9: 395-409. https://doi.org/10.1007/s10518-010-9208-4

Erberik, M. A. 2008a. "Generation of fragility curves for Turkish masonry buildings considering in-plane failure modes", Earthquake Engineering and Structural Dynamics, 37: 387–405. https://doi.org/10.1002/eqe.760

Erberik, M. A. 2008b. "Fragility-based assessment of typical mid-rise and low-rise RC buildings in Turkey", Engineering Structures, 30: 1360–1374. https://doi.org/10.1016/j.engstruct.2007.07.016

Gülerce, Z., Kargıoglu, B., Abrahamson, N. A. 2016. "Turkey-adjusted NGA-W1 horizontal ground motion prediction models". Earthquake Spectra, 32: 75–100. https://doi.org/10.1193/022714EQS034M

i4Works 2023. "SiteEye: Cloud-based Photogrammetry and Project Management", [Computer Software]. Available from: https://siteeye.co [Last accessed on February 13, 2023]

Kale, Ö., Akkar, S., Ansari, A., Hamzehloo, H. 2015. "A ground-motion predictive model for Iran and Turkey for horizontal PGA, PGV and 5%-damped response spectrum: Investigation of possible regional effects". Bulletin of the Seismological Society of America, 103: 963–980. https://doi.org/10.1785/0120140134

Kale Ö. 2019. "Some discussions on data-driven testing of Ground-Motion Prediction Equations under the Turkish ground-motion database. Journal of Earthquake Engineering, 23: 160–81. https://doi.org/10.1080/13632469.2017.1323047

Konno, K., Ohmachi, T. 1998. "Ground-motion characteristics estimated from spectral ratio between horizontal and vertical components of microtremor". Bulletin of the Seismological Society of America, 88: 1: 228–241. https://doi.org/10.1785/BSSA0880010228

Kotha, S.R., Weatherill, G., Bindi, D., Cotton, F. 2022. "Near-source magnitude scaling of spectral accelerations: analysis and update of Kotha et al. (2020) model", Bulletin of Earthquake Engineering, 20: 1343–1370. https://doi.org/10.1007/s10518-021-01308-5

Nakamura, Y. 1989. "A method for dynamic characteristics estimation of subsurface using microtremor on the ground surface". QR of Railway Technical Research Institute, 30: 25-33.

Nogoshi, M., Igarashi, T. 1971. "On the amplitude characteristics of microtremors". Journal of the seismological society of Japan, 24: 24-40 (in Japanese with English abstract).

Pizzaro 2017. "HOVSR (Version 2.0)". https://github.com/ppizarror/HOVSR [Downloaded on February 02, 2023]

Turkish Accelerometric Database and Analysis System (AFAD TADAS). Disaster and Emergency Management Presidency, Department of Earthquake, Ankara, Türkiye. https://tadas.afad.gov.tr/map [Last accessed on February 19, 2023].

Turkish Building Earthquake Code (TBEC) 2019. Ministry of Interior, Disaster and Emergency Management Presidency (AFAD), Ankara, Turkey.